Rep. Prog. Phys. **61** (1998) 431–482. Printed in the UK PII: S0034-4885(98)21753-2

Superconducting cavities for accelerators

Dieter Proch
Deutsches Elektronen–Synchrotron DESY, Notkestrasse 85, 22603 Hamburg, Germany

Received 11 November 1997

Abstract

Superconducting cavities have been in operation in accelerators for 25 years. In the last decade many installations in storage rings and linacs have been completed. Meanwhile, nearly 1 km of active cavity length is in operation in accelerators. Large-scale applications of superconducting radiofrequency systems are planned for future e^+e^- linear colliders and proton linacs.

Superconducting cavities have been proved to operate at higher gradient, lower AC power demand and more favourable beam dynamics conditions than comparable normal conducting resonators. The performance of the best single-cell cavities comes close to the intrinsic limitation of the superconducting material. Complete multicell structures with all auxiliaries (couplers, tuner, etc) lag behind in performance because of their complexity.

In this paper, an overview of accelerators with superconducting cavities is given. Limitations of superconducting performance are described and research and development efforts towards understanding and curing these effects are discussed in detail. Fundamentals of superconductivity and radiofrequency cavity design are briefly explained.

0034-4885/98/050431+52$59.50

Contents

		Page
1.	Introduction	433
2.	Operating systems	434
	2.1. Operating superconducting accelerators	434
3.	Projects under development/installation	440
	3.1. Superconducting cavities in the LEP e^+e^- collider	440
	3.2. Superconducting cavities for TESLA	441
	3.3. High-current cavities	443
4.	Research and development projects	445
	4.1. Thin-film technology	445
	4.2. High gradients	449
	4.3. Field emission studies	452
	4.4. New materials	456
5.	General design criteria	457
	5.1. Comparison between normal conducting (NC) and superconducting (SC) accelerating cavities	457
	5.2. Optimum gradient	459
	5.3. Optimum temperature	460
6.	Fundamentals of RF superconductivity	463
	6.1. Surface resistance	463
	6.2. Critical field	466
	6.3. Experimental limitations of the surface resistance	467
	6.4. Experimental limitations of the accelerating gradient	468
	6.5. Diagnostic methods for superconducting cavities	473
7.	Fundamentals of cavity design	474
	7.1. Principal cavity layout	474
	7.2. Shunt impedance, Q and R/Q value	478
	7.3. Optimization considerations	479
8.	Conclusion	480
	Acknowledgments	481
	References	481

1. Introduction

Usually the energy of charged particles is increased by interaction with the electric component of a radiofrequency field. The frequency might range from 50 MHz to above 10 GHz, depending on the phase velocity of the particles and on geometric considerations. The so-called accelerating structure guides the electromagnetic fields. To first order, the cross section of the structure scales inversely with the operating frequency, whereas the longitudinal shape is optimized for highest exchange of energy. An important parameter is the energy gain per single passage (of a single charged particle) and it is measured in MeV per metre of accelerating structure. In many cases, the gradient of the accelerating voltage is given instead: E_{acc} (MV m^{-1}). The metallic boundary condition of the accelerating structure causes radiofrequency surface currents; the surface currents produce loss which is proportional to the resistivity of the metal. Therefore, a high-conductivity metal is chosen to keep these losses small, but even for copper as the material of the accelerating structure, the loss in the metallic walls is the dominant part of the radiofrequency power which has to be supplied by the generator. The second part is the so-called beam power, which is the product of the average beam current times the accelerating voltage. As a rule of thumb, a normal conducting accelerating structure for electrons will dissipate around 100 kW per metre and produce an accelerating gradient of $E_{\mathrm{acc}} \leqslant 2$ MV m^{-1}. This is already the maximum accelerating gradient obtainable in normal conducting structures because of inherent difficulties in cooling the structure. One solution to reach higher accelerating gradients is to pulse the accelerating field and thus to reduce the average wall power loss. The drawback is that high peak radiofrequency power is needed so that the pulse length must be very short.

Parallel to the development of superconducting cables for magnets, research and development effort was launched in the late 1960s towards the use of superconducting material for radiofrequency accelerating structures. In both cases, the high critical field of suitable superconductors permits operation at field levels which are above the values of a comparable normal conducting design. In the case of niobium for superconducting accelerating structures, gradients up to 57 MV m^{-1} should be possible (see also table 4 later). There are other superconductors, Nb_3S_n for example, which could allow even higher gradients. The main advantage of superconducting accelerating structures is the fact that they enable high gradients under continuous wave operation. It should be noted, however, that in contrast to DC superconducting magnets the radiofrequency currents produce losses which have to be cooled by a refrigerator, but the overall efficiency of a superconducting radiofrequency system is still higher than that of a comparable normal conducting system.

Another important advantage of superconducting structures is the fact that there is more freedom in designing the shape of the accelerating cavity. Normal conducting cavities have to be shaped to produce minimum radiofrequency loss. A superconducting structure produces very low radiofrequency losses. Therefore, the shape of the structure can be optimized for other properties. Energy exchange occurs from the beam to the accelerating structure which might deteriorate the quality of the beam. This effect scales with the beam current and thus becomes more critical in high current accelerators. With superconducting structures a shape can be chosen which has less beam-to-cavity interaction and which allows the acceleration of higher currents without reduction of the beam quality.

At present, the operating accelerating gradient of a superconducting system is not higher than 15 MV m^{-1}. There are two major limitations: thermal instabilities (also called 'quenches') and field emission. In the first case, normal conducting defects in the surface produce heat and finally drive the superconductor above the critical temperature. In the

second case, field emitted electrons from the inner cavity surface are accelerated by the electric fields. They will impact the superconducting surface and produce excessive heat.

Large progress has been made in the last few years in analysing and understanding these effects. Improved preparation and cleaning techniques have resulted in a measured performance of short accelerating structures close to the theoretical limit. There are many laboratories which are active in the development and application of superconducting cavities for the acceleration of electrons, positrons and heavy ions. Within the framework of an international collaboration, considerable effort in research and development was launched to further develop the superconducting cavity technology and thus establish the industrial basis for a possible large-scale superconducting linear collider in the TeV energy range [1].

In this paper the main activities in the field of superconducting cavities are described, the present knowledge of understanding is presented and fundamental physics and technology are briefly discussed. Detailed information can be found in the related references; an overview over the field of superconducting cavity technology for accelerator application is given in [2].

2. Operating systems

2.1. Operating superconducting accelerators

The phase velocity $v = \beta \cdot c$ of an accelerating structure (strictly speaking, the phase velocity of the electromagnetic wave in the accelerating structure) must be equal to the speed v of the particle to be accelerated. Electrons reach 99.9% of the speed of light c ($\beta = v/c$ equals 0.999) at an energy of 12 MeV. Practically all the gain of energy is converted into an increase of mass above this value according to relativistic kinematics. Therefore, an electron accelerator consists of structures with $\beta = 1$, with the exception of a very short capture section just behind the electron gun.

The velocity of a relativistic particle is determined by its energy, measured in units of its rest mass. Therefore, the heavy proton needs a higher energy by a factor of nearly 2000 to reach the same velocity as the light electron (the mass ratio is nearly 2000). As a consequence, proton accelerators require much longer sections with variable phase velocity.

2.1.1. Accelerating structures with phase velocity $\beta = 1$. Accelerating structures with $\beta = 1$ consist of a round pipe which is intercepted by equally spaced discs (see figure 1).

Table 1. Accelerators for electrons with superconducting structures ($\beta = 1$).

Laboratory	Operational	Frequency (MHz)	Active length (planned) (m)	Average gradient (planned) (MV m^{-1})	Average current (mA)
Stanford HEPL, Recyclotron [10]	1972	1300	6	2–3	0.5
University of Illinois, MUSL [11]	1972–92	1300	6	2–3	0.01
CERN, SPS [8]	1987	352	5.1	5.5	0.5
KEK, TRISTAN [3]	1988–94	508	48	3.0–4.7	14
Darmstadt, S-DALINAC [12]	1990	2997	10.25	5	0.04
DESY, HERA [4]	1991	500	19.2	2	35
CEBAF [5]	1996	1497	169	5	0.4
CERN, LEP [7]	1997	352	340 (462)	(6)	4

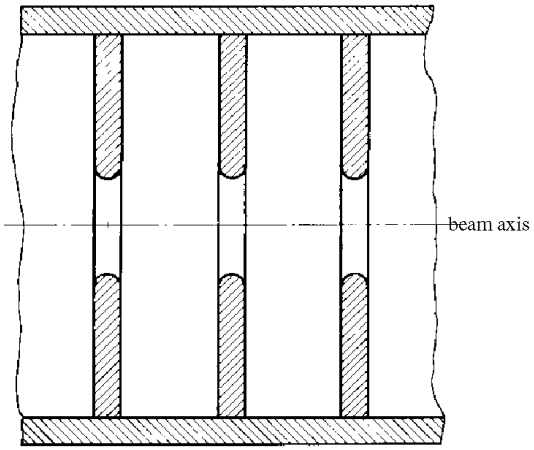

Figure 1. Cross section of a typical disc loaded waveguide. The diameter of the outer pipe determines the resonance frequency, the distance between the discs adjusts the phase velocity of the electromagnetic wave and the diameter of the iris opening mainly influences the beam–cavity interactions.

The distance between the discs determines the phase velocity of the electromagnetic wave. It is equal to half the wavelength of the operating frequency in a typical superconducting design. There is a hole in the middle of the disc for passing the beam current. The diameter of the hole (iris diameter) is chosen so as to be able to adjust some local microwave properties, whereas the diameter of the pipe determines the resonance frequency of the accelerating structure. The unit of two adjacent discs and the intermediate tube is named a cell. A combination of N cells forms the accelerating structure which is powered by one input coupler. This N-cell structure is also named an N-cell cavity. Most superconducting cavities consist of less than 10 cells.

Superconducting cavities in the TRISTAN storage ring at KEK [3]. KEK is a national Japanese laboratory for high-energy physics. In the early 1980s it was decided to upgrade the energy of the TRISTAN e^+e^- storage ring by installation of 32 superconducting cavities (in addition to 104 normal conducting resonators). The production, assembly and installation of the superconducting cavities were carried out mainly by industrial firms. The cavities were fabricated from niobium sheets by spinning, electron beam welding, electro-polishing and heating at 800 °C. The heat treatment was needed to clean the Nb from hydrogen which was picked up during electro-polishing. Two five-cell cavities are housed in one cryostat (see figure 2).

The superconducting cavities were operated at a gradient between 3 and 4.7 MV m^{-1}. The performance (maximum accelerating field and radiofrequency losses) did not deteriorate during seven years of operation. The major reasons for the lower gradient were fast quenches in some cavities during routine accelerator operation. There is evidence that synchrotron radiation from the bending magnets in the arcs released absorbed gases from the cold cavity surfaces. These gases initiated a local plasma discharge. In 1995 the high-energy physics runs at TRISTAN were finished. It is planned to convert the accelerator into a B-factory installation. The possible use of superconducting cavities of a new design (for high-current application) is under investigation.

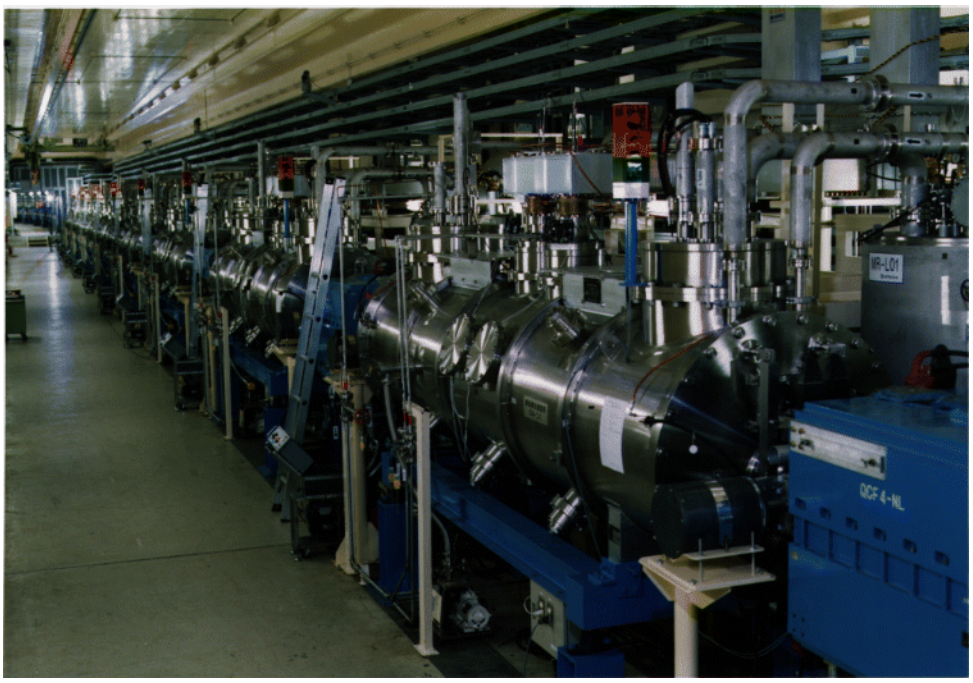

Figure 2. A photograph of the superconducting accelerating system at KEK (National Institute of High-Energy Physics, Tsukuba, Japan) [3]. In total, 32 superconducting cavities were installed in the storage ring for electrons (TRISTAN). Each cryostat houses two five-cell cavities (508 MHz). In the picture the vacuum vessel of the cryostat can be seen. The cryogenic supply (liquid nitrogen and helium) is fed from the top, the rectangular waveguide for transmitting the radiofrequency power can be identified in the middle region of the cryostat vessel. The cryogenic valve boxes are placed behind the accelerating cryostats.

Superconducting cavities in the HERA storage ring at DESY [4]. HERA is a storage ring facility used to collide 820 GeV protons with 27 GeV electrons. The radiofrequency system of the electron ring consists of 82 normal conducting and 16 superconducting cavities. The superconducting cavities were produced by industry (spinning of cups from Nb sheets, electron beam welding, tumbling and chemical cleaning) whereas the assembly and installation were carried out by DESY staff in 1992 (see figure 3). The average gradient of the installed cavities was 5 MV m^{-1}. At the design current of 60 mA the maximum gradient is limited to 2 MV m^{-1} by the maximum radiofrequency power of 100 kW per cavity.

Superconducting cavities at CEBAF [5]. CEBAF (Continuous Electron Beam Accelerator Facility) is a recently founded laboratory for nuclear physics research. It is situated at Norfolk, Virginia, USA. Electrons are accelerated to an energy of up to 4 GeV. Key performance characteristics are the energy resolution of 10^{-4} and the continuous wave operation. The accelerator was commissioned in 1995 and physics runs started in 1996.

The accelerator consists of two superconducting linacs with four magnetic bends for recirculation of the beam. Two cavities are placed in one helium vessel (see figure 4), four

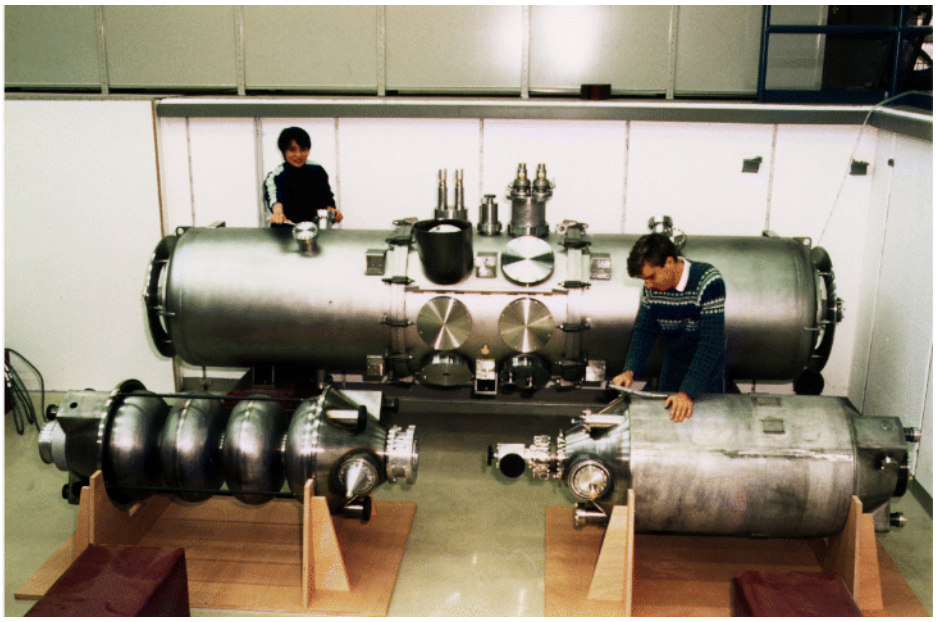

Figure 3. 'Assembly' photograph of the superconducting accelerating system for the HERA (Hadron Electron Ring Accelerator) storage ring at DESY [4]. In the foreground the four-cell niobium cavity (500 MHz) can be seen before (left-hand side) and after (right-hand side) closing the vessel for the liquid helium. In the background the vacuum vessel of the cryostat can be seen. The input coupler for the radiofrequency power will be assembled at the two large centre flanges, and the cryogenic lines (for liquid and gaseous helium) will be attached to the four top valves.

of those vessels being housed in one cryostat. The cavities are formed from Nb sheets and were fabricated by industry. The final cleaning, testing and installation were carried out by CEBAF staff. The average accelerating gradient during the acceptance test was 6.8 MV m^{-1} as compared to 5 MV m^{-1} as specified. In the accelerating tunnel each cavity is operated by one 5 kW klystron, so that it can be controlled individually.

2.1.2. Accelerating structures with phase velocity $v < 1$. Protons and heavy ions need an accelerating structure with a relative velocity $\beta = v/c < 1$. Due to acceleration the velocity will change along the linac. In the case of accelerating structures for electrons, the phase velocity is adjusted by the distance between discs in the accelerating tube. The distance equals half a wavelength in a typical superconducting design; this design is very ineffective for a small particle velocity. Therefore, other methods are applied to slow down the phase velocity of the electro-magnetic wave.

'Helix' design. In this design a coil is placed inside the accelerating tube (see figure 5). The coil is oriented so that its axis coincides with the beam axis. The radiofrequency current flows along the windings of the coil. The phase velocity of the electric field on the axis is reduced to the ratio of the pitch to circumference of the coil winding. Therefore, the phase velocity can be adjusted by changing the pitch. This so-called helix design has been used in

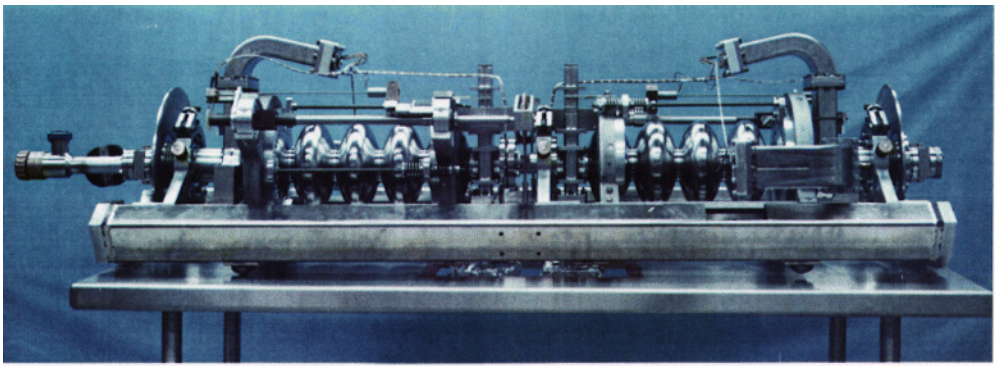

Figure 4. The CEBAF (Continuous Electron Beam Accelerator Facility, Norfolk, Virginia, USA [5]) superconducting cavity pair at the stage of assembly in the clean room. Two five-cell cavities (1.5 GHz) are grouped in one helium vessel, four of those being housed in one vacuum vessel. Both bend waveguides on either end act as absorbers for beam-induced radiofrequency power, and the input power is fed via the two reduced side vertical waveguides in the centre. The rods and flanges around both cavities belong to the cold tuning mechanism for the resonance frequency of the cavities.

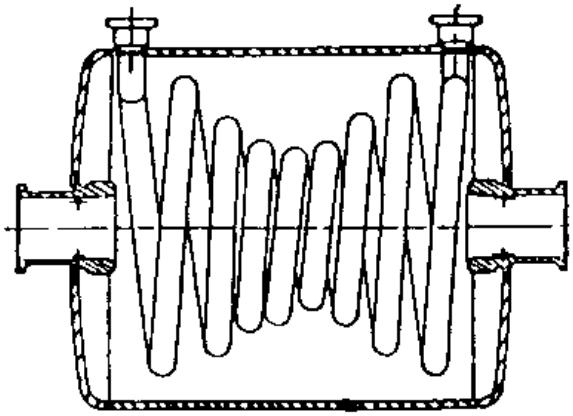

Figure 5. Cross section of a helix resonator for acceleration of particles with low velocity ($\beta < 1$) [6]. The phase velocity of the electric field on the axis is reduced according to the ratio of the pitch to circumference of the coil winding. In the example shown, the winding diameter is not constant in order to enhance the mechanical stability of the helix.

the early fabrication of low-β resonators. A severe drawback is the mechanical weakness of the coil; vibrations will be transformed into changes of the resonance frequency. Attempts have been made to compensate for this effect by switching external capacitances. In practice, however, it was not possible to operate the system stably under all conditions. Another method is to mechanically strengthen the coil by a thicker pipe diameter or by varying the coil diameter and thus modulating the mechanical resonance frequency. Although such a design was successfully operated at Saclay [6], the helix design is no longer in use.

'Split ring' design. Here the coil is reduced to one winding. Two small drift tubes at both ends of the winding form an additional capacitor (see figure 6). The 'split ring' is mechanically fixed in the middle of the winding by a post to the outer cylinder. The phase velocity of this structure can also be changed to some extent by the pitch of the split ring. The 'split ring' design is mechanically stable enough to operate with the help of a fast tuner. This design is under operation at different laboratories (see table 2).

Figure 6. A photograph of the split ring resonators for the ATLAS accelerator for heavy ions (Argonne National Laboratory, Argonne, Illinois, USA [13]). The beam passes through the hole of the two cylinders in the centre (drift tubes). The accelerating field is established between both drift tubes (centre field) and the end plates (not assembled in the photograph) and each drift tube (end fields). The outer housing is made from niobium clad copper to enable cooling by conduction. The inner loop and drift tubes are fabricated from niobium tube and sheet material and are filled with liquid helium for cooling.

Quarter-wave resonator. A coaxial line can be used as a resonator by placing a short or an open end on either end of the line. The shortest resonator is the so-called quarter-wave design with one end shorted and the other end open (length of coax is one quarter wavelength). The diameter of the coax line (and thus the gap distance between the inner and outer coaxial tube) does not influence the resonance frequency, it is only determined by the length of the coax line. The electric field pattern in a coax line (operated in the fundamental mode) is radial. Therefore, a longitudinal electric field is experienced by a particle which travels perpendicular to the axis of the coax geometry (see figure 7). In practice the beam

Table 2. Accelerators for heavy ions with superconducting structures ($\beta < 1$).

Institution (operational since)	Cavity type	Frequency (min/max) (MHz)	Optimum velocity (min/max)	Total number of cavities
Argonne National Laboratory [13] (1978)	Nb split-ring/Nb interdigital	48.5/145.5	0.023/0.160	74
Stony Brook [14] (1983)	Pb/Cu split-ring Pb/Cu quarter-wave	150	0.055/0.100	42
Florida State University [15] (1987)	Nb split-ring	97	0.065/0.105	14
University of Washington [16] (1987)	Pb/Cu quarter-wave	148.9	0.10/0.20	37
CEN Saclay [6] (1989)	Nb helix	81/135	0.085	50
JAERI [17] (1994)	Nb quarter-wave	129.8	0.10	44
INFN Legnaro [18] (1995)	Pb/Cu quarter-wave Nb quarter-wave Nb/Cu quarter-wave	80/160	0.055/0.11	64
ANU Canberra [19] (1997)	Pb/Cu split-ring	150	0.100	10

pipe is placed near to the open end of the coax resonator to have maximum electric field gain and to avoid the influence of the magnetic field (which has its maximum at the shorted end). The phase velocity of the accelerating electric component can be adjusted by the gap distance between the inner and outer coax tube at the location of the beam pipe. The gap must be shorter for a slower particle because it must leave the gap before the voltage changes sign. Therefore, a design with more than two gaps in one quarter-wave resonator is desirable for very-low-β applications. This is achieved by the 'indigital line' resonator. It is a variation of the quarter-wave resonator by splitting the end of the inner conductor like a fork. The necessary phase reversal is forced by a second indented fork which is grounded to the outer conductor.

Low-β resonators have been made by plating Pb on Cu, by welding bulk Nb or Nb-clad Cu or by sputtering Nb onto Cu. The lead plating technology is considered to be a low-cost fabrication method. However, lead-plated resonators produce more radiofrequency losses as compared to Nb resonators. Therefore, this technology is restricted to low-field applications. Low-β resonators made from bulk Nb or from Nb-clad Cu (done by explosive bonding Nb sheets with Cu sheets) show similar behaviour. The advantage of Nb-clad Cu is that cooling can be done by heat conduction through the Cu, whereas bulk Nb needs a liquid helium container. Even better cooling can be achieved for sputtered Nb on Cu. The sputtered Nb film has a typical thickness of 10 μm whereas the Nb-clad Cu needs a Nb thickness in the order of several millimetres. However, effort is needed to produce a high-quality Nb sputtered film on complex geometries.

3. Projects under development/installation

3.1. Superconducting cavities in the LEP e^+e^- collider

In the first stage the accelerating system of the LEP storage ring consists of normal conducting cavities (352 MHz). To upgrade the energy from 45 GeV to 96 GeV, 272 superconducting four-cell cavities will be installed to the remaining 84 normal conducting resonators [7] (see figure 8). With the exception of the first 20 cavities, the superconducting resonators were not made from solid Nb material but by sputtering Nb onto Cu. Two major arguments are quoted in favour of this technology: cost saving by the reduced amount of

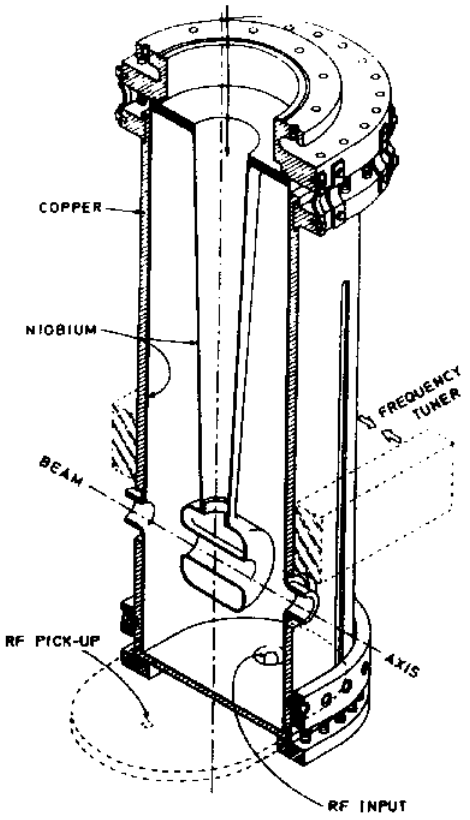

Figure 7. The quarter-wave resonator for acceleration of particles with low velocity ($\beta \simeq 0.1$) [17]. The coaxial resonator is excited in the lowest resonant mode (quarter wave). The accelerating particle crosses the resonator at the area of the highest electric field.

Nb material (a 2 μm layer instead of a 4 mm thick sheet) and stabilization of a thermal instability (quench) of the superconducting cavity by the high thermal conductivity of Cu. The technology of sputter-coating large surface areas was developed at CERN during the 1980s and then transferred to industry. After a learning process the cavity fabrication reached a high standard. The specified value of the accelerating gradient of 6 MV m^{-1} could be guaranteed with one sputter coating in most cases. The commissioning of the complete system is scheduled for 1998.

It is worth noting that four superconducting resonators of the LEP design have been in operation in the SPS storage ring since 1989 [8]. They are equipped with a fast feed forward to control the cavity voltage. This allows electron acceleration but also a detuning to lower the impedance of the superconducting resonator during proton acceleration.

3.2. Superconducting cavities for TESLA

Within the frame of an international collaboration, a development project was launched to explore the feasibility of the superconducting linear collider TESLA (TeV Energy Superconducting Linear Accelerator) [1]. The TESLA Test Facility (TTF) at DESY [9]

Figure 8. Assembly of the superconducting accelerating module for the LEP storage ring (CERN, Geneva, Switzerland [7]). Four four-cell cavities (352 MHz) are grouped in one cryostat. The resonators are made from copper and are plated with a thin Nb layer (some μm) by sputter technology. The vacuum vessel is constructed by a thin outer sheet cover held in place by an inner support structure, thus allowing easy access to all inner parts during assembly. The rods bridging the cavity are used to adjust the cavity length and thus the resonance frequency. The length of the rods is controlled by thermal expansion (course tuning) and magneto-striction (fine tuning). The cryogenic and radiofrequency power lines are attached to the cryostat from the top (the tilt angle against the vertical is due to space restrictions in the tunnel).

incorporates the necessary infrastructure to treat high-gradient superconducting cavities, as well as the installation and operation of an experimental superconducting accelerator with 500 MeV beam energy. The nine-cell cavities are made from Nb sheet material and resonate at 1.3 GHz (see figure 9). They are treated by an automated chemical system under clean room conditions and are processed by high-pressure water and/or by high-radiofrequency power conditioning. Eight cavities are grouped in one cryomodule, four of these modules are needed for the first test accelerator (see figures 10 and 11). The key development target is to operate the experimental linac at a gradient of 15 MV m^{-1} and to upgrade the cavity performance to the TESLA design value of 25 MV m^{-1}. One of the first TTF nine-cell cavities has already reached the TESLA design goal in the first acceptance test (see figure 12). A second development goal is to simplify the cavity design and fabrication techniques in order to reduce the investment costs of a possible TESLA installation.

3.3. High-current cavities

The effectiveness of colliding beam accelerators is the rate of interesting physics events. This rate is proportional to the luminosity L,

$$L \propto \frac{N^2 f_{\mathrm{rep}}}{\sigma_x \sigma_y} \tag{1}$$

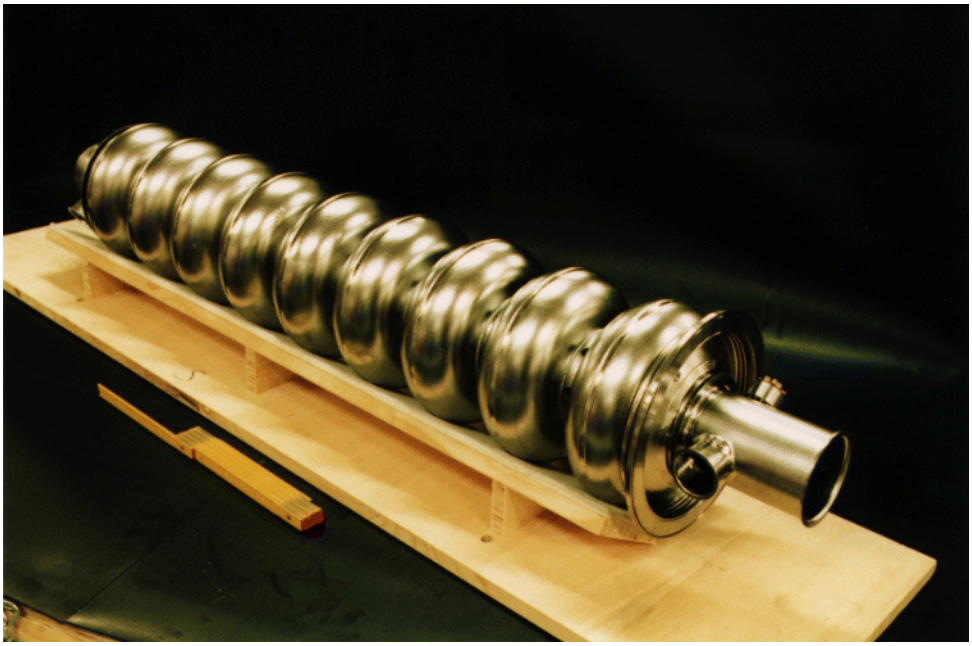

Figure 9. A photograph of the nine-cell niobium resonator for the TESLA Test Facility, TTF [9]. The cavity is made by deep drawing of Nb sheets (2.8 mm) and EB welding at the iris and equator. At the right beam port the opening for the input coupler can be seen. At a later stage of production, the Ti tank for the liquid helium is welded to the cavity (see the bellow and flange at the right beam port).

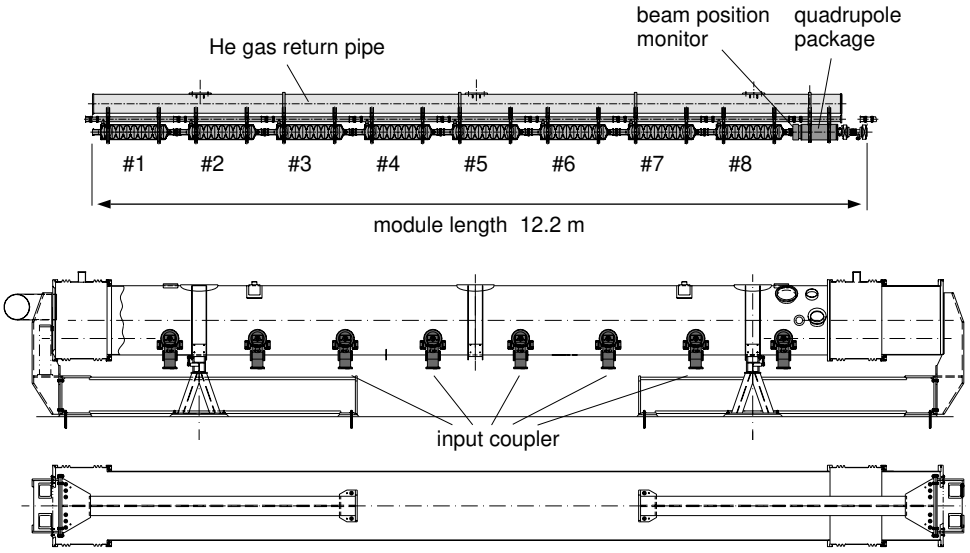

Figure 10. A longitudinal cut of one module for the TTF linac (Tesla Test Facility, TeV Electron Superconducting Linear Accelerator [1]). Eight nine-cell cavities (1.3 GHz) are grouped in one module. The modules will be connected by large bellow sleeves, so that a long (several 100 m) unit with common vacuum and cryogenics will be established in the TESLA linac.

where σ_x (σ_y) is the dimension of the bunch in the horizontal (vertical) direction, N the number of particles per bunch and f_{rep} the bunch collision frequency.

There are two principal ways of improving the luminosity:

- decreasing the cross section of the bunch size or
- increasing the number of particles per pulse.

The first method results in demanding requirements of focusing and beam steering technologies at the interaction region. The second method asks for higher beam current in the accelerator. The typical design current for high-current e^+e^- storage rings (so-called factories for phi-, tau-charm- and B-particles) or for the large hadron collider (LHC) is in the order of 1 A as compared to around 50 mA in storage rings for high-energy physics. Difficulties like beam instabilities arise from high currents passing through the radiofrequency cavity. Under these conditions the major advantages of a superconducting against a normal conducting radiofrequency system are as follows.

- The shape of a superconducting cavity is favourable for a low beam–cavity interaction (see section 5.1). This is demonstrated in figure 13. The iris diameter can be made larger by a factor of two. The beam cavity interaction scales with the fourth power of this diameter so that a large reduction is gained.
- The accelerating gradient in a superconducting cavity under continuous wave operation can be larger by more than a factor ten. Therefore, less cavities are needed to produce the same amount of total accelerating voltage.
- At higher gradients more radiofrequency energy is stored in the cavity. As a consequence, the cavity system is less sensitive to 'distortions' by the beam current.

The interaction of the high beam current with the accelerating cavity might lead to current instabilities. This can happen under continuous wave conditions if a critical beam current is surpassed or also under transient conditions, for example during injection. In both

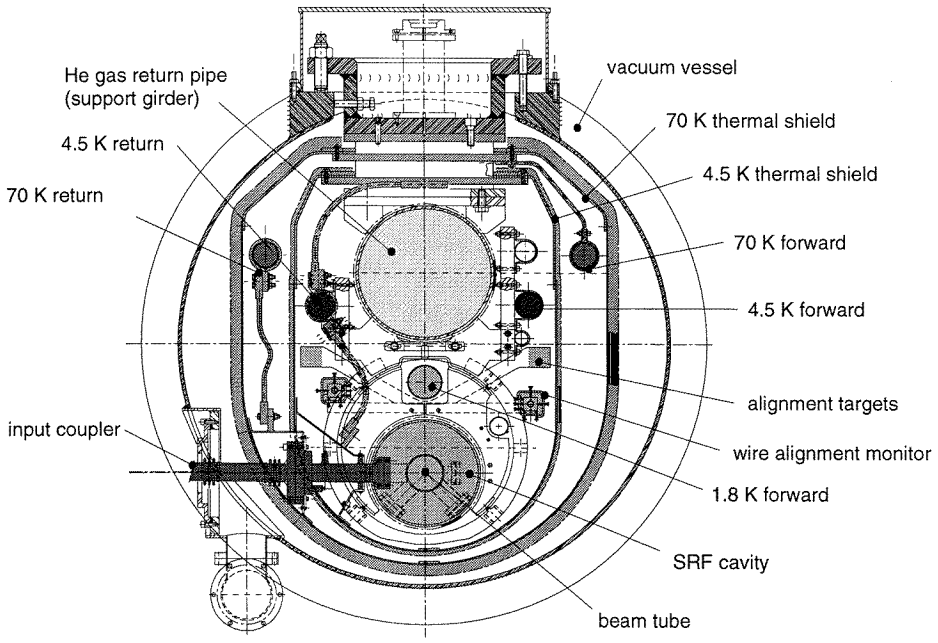

Figure 11. Cross section of the TTF superconducting accelerating module [1]. The upper large diameter pipe is the supply line for the helium and is also used as the mechanical support for the cavities (nine-cells, 1.5 GHz). The outer vacuum vessel holds the inner cavity/cryo system by three hanging posts. The cavity and its helium vessel is mounted below the helium pipe. Eight cavities are grouped in one module (see figure 10).

cases the effect is proportional to the strength of the beam–cavity interaction but inversely proportional to the stored radiofrequency energy in the cavity. As pointed out above, the superconducting cavity design is beneficial in both aspects. In addition, the total amount of beam–cavity interaction strength is smaller because of the lower number of cavities needed.

The high beam current requires a high radiofrequency power per cavity. Therefore, an input coupler has to be developed to withstand up to 500 kW as compared to less than 100 kW for a high-energy physics storage ring design. The high beam current will also result in a considerable increase of induced higher-order mode power in the accelerating cavity. Therefore, an efficient damping scheme is needed, but the power should not be dissipated at cryogenic temperatures. One elegant solution is to enlarge the diameter of the beam pipe to such an extent that all frequencies above the accelerating mode are propagating to the warm end of the beam pipe. Such a design was developed at Cornell (see figure 14) and KEK. It should be noted that it is a single-cell cavity, being powered by one radiofrequency input coupler. Therefore, the radiofrequency input power can be kept at a manageable level.

4. Research and development projects

4.1. Thin-film technology

The superconducting surface current flows in a very thin surface layer of typically less than 100 nm. Therefore, one can produce a cavity from normal conducting material. In a second

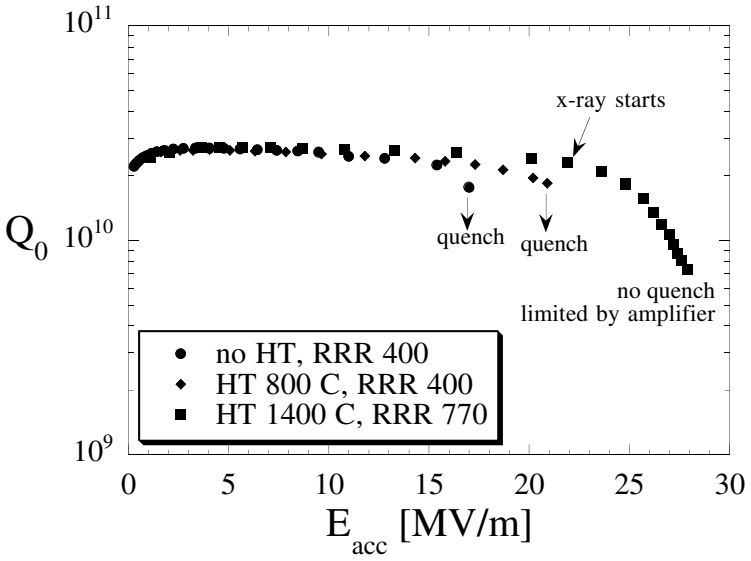

Figure 12. Performance of a nine-cell cavity for the TESLA Test Facility TTF [9]. The quality factor Q_0 is measured as a function of the accelerating field E_{acc} under continuous wave operation. The maximum gradient improved after heat treatment (HT) at 800 °C and 1400 °C. The thermal conductivity λ of the Nb, and thus the RRR (residual resistance ratio; RRR $\simeq 4\lambda_{(4.2\,K)}$) value, too, improved after 1400 °C heat treatment. This cavity meets the specification for TESLA [1]: $E_{acc} = 25$ MV m^{-1} at $Q_0 = 5 \times 10^9$.

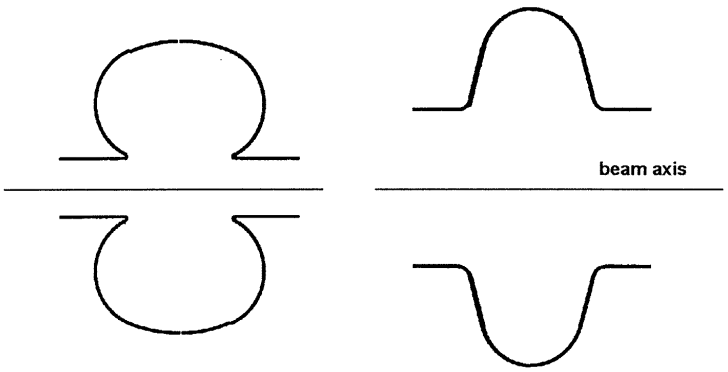

Figure 13. Typical cross section of a normal conducting (left) and superconducting (right) single-cell cavity for high-current application. In the normal conducting case the shape must be optimized to reduce the radiofrequency dissipation. This is done by the so-called 'nose cone' design which produces high electric fields near to the beam axis by reducing the beam pipe diameter and placing sharp corners at its end. In the superconducting design the radiofrequency dissipation is very small, so that a less efficient shape with a large diameter of the beam pipe can be afforded. This has considerable benefits in reducing beam-induced voltages.

step, the radiofrequency side is coated with a superconducting film. The advantages of this method are as follows.

- The vacuum body can be produced from standard material. Copper is a good candidate because of its high thermal conductivity.
- The superconducting layer can be very thin (some micrometres). Therefore, a

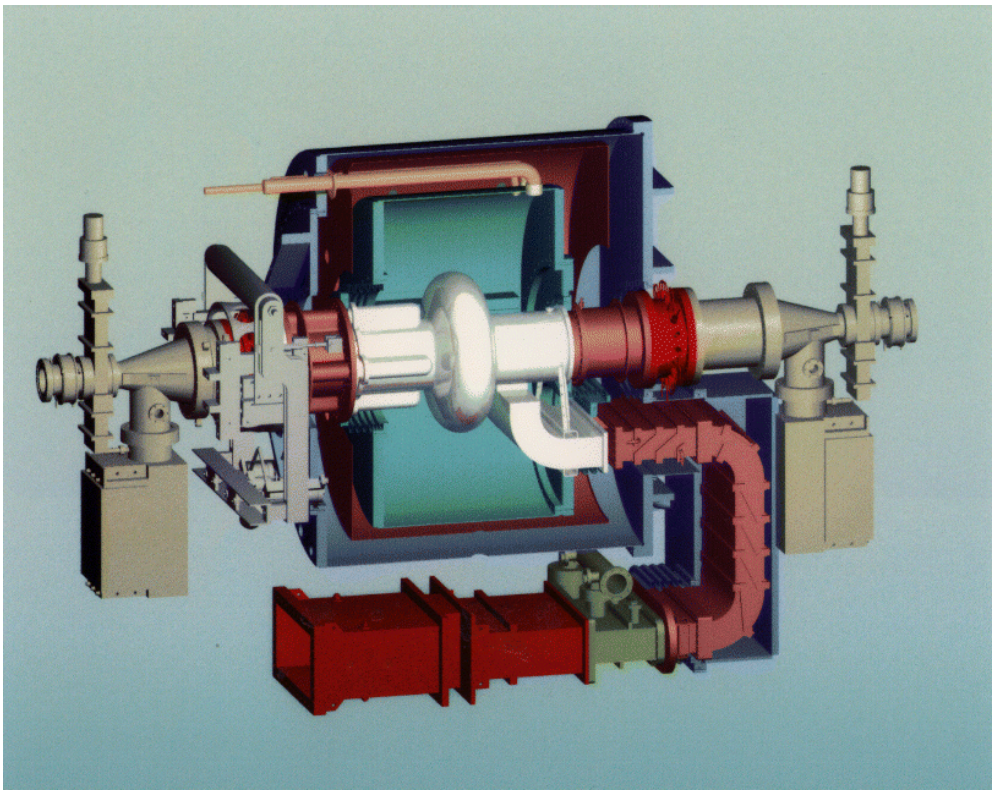

Figure 14. 3D picture of a typical single-cell superconducting cavity module for high-current application (Cornell design [43]). Challenging design parameters are the high radiofrequency power of 500 kW per cavity (because of the high beam current of 500 mA) and the excessive beam-induced high-frequency power of several kilowatts. This power is transmitted through the large beam pipes at either side of the cavity and is absorbed by a dissipative coating at room temperature.

low thermal conductivity of the superconductor is no longer critical in avoiding thermal instabilities. In addition, it is a cost saving argument for expensive superconductors, especially for large resonators at low frequencies.

- A compound superconductor can be produced by appropriate coating methods (e.g. by co-evaporation). This is an important advantage, if bulk material of the right size is not available.

4.1.1. Nb–Cu sputtered cavities. The sputter technique for coating Cu resonators with a film of Nb has been explored over many years at CERN [20]. Magnetron sputtering proved to produce better Nb layers than diode sputtering. A high surface quality of the Cu resonator (no cracks at the weld, no surface pits, no chemical residues on the surface) is necessary to produce a perfect Nb film. The coating technology has been transferred to industry. However, it took several years of industrial production experience to reach good coatings in one try. In the spring of 1997 more than 150 cavities (four-cell, 352 MHz) have been accepted. They reached the specified accelerating gradient of 6 MV m^{-1} at a quality factor of 3×10^9.

The thermal conductivity of a sputtered Nb film is about a factor of 20 lower than that of bulk niobium. It is mainly due to a too high oxygen content in the Nb layer. The thickness of the sputtered film is 2 μm instead of 3 mm for bulk Nb resonators. Therefore, the resulting temperature gradient across the sputtered film is still lower than in the equivalent bulk Nb wall.

At low accelerating fields, the Q-value of a sputtered resonator is higher than in a bulk Nb resonator. The surface resistance of a superconductor depends on material parameters and can be calculated by the Bardeen–Cooper–Schriefer (BCS) theory of superconductivity [34]. It is astonishing that the lowest surface resistance is not given at the cleanest state of the material. In this sense, the enhanced oxygen content of the sputtered Nb film is advantageous for the low value of the surface resistance.

All sputtered Nb–Cu resonators exhibit a more than quadratic increase of radiofrequency losses when raising the cavity field (i.e. the measured Q-value drops down when raising the stored energy in the cavity; so-called 'Q-slope'). In the case of the Nb–Cu cavities for LEP, the high Q-value of a sputtered cavity intercepts the bulk resonator curve at around 6 MV m^{-1} (see figure 15). Therefore, sputtered Nb–Cu resonators loose their attractiveness for high-gradient application. The nature of the additional loss in sputtered films is under investigation at several laboratories. It is observed that sputtered films show a density of defect locations higher by three orders of magnitude (dislocations, point defects, etc). The favoured explanation of the additional radiofrequency loss is that magnetic flux penetrates at these defects and produces loss in its normal conducting core. There is hope that these defects can be cured by improved fabrication technologies.

4.1.2. Nb_3Sn cavities. Nb_3Sn exhibits a high T_c of 18 K and a thermodynamic field of 400 mT. In comparison to niobium, the same low surface resistance is already reached at a temperature higher by a factor of two (see equations (10) and (12), section 6.1). Furthermore, the high critical field promises high-gradient application. Nb_3Sn layers can be obtained by diffusion of Sn vapour into bulk niobium at a temperature around 900 °C. The difficulty is

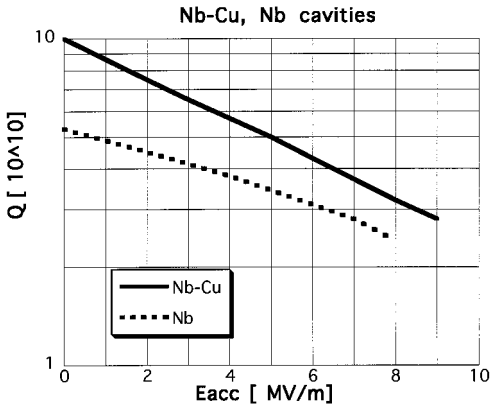

Figure 15. Comparison of the typical performance of Nb-coated Cu cavities and bulk Nb cavities at CERN [20]. At low gradient the Q-value of Nb–Cu cavities is considerably higher than that of cavities made from bulk Nb. At higher gradient this advantage is reduced by increasing radiofrequency losses at grain boundaries of the sputtered film. The higher Q-value of the sputtered film is explained by the material and lattice dependency of the superconducting resistance $R_{BCS}(R_{BCS} \propto 1/Q)$ [34].

to avoid the growth of the other non-superconducting phases, which exist near to the exact stoichiometry in the phase diagram. Recently, it was demonstrated [21] that the CEBAF specification of 5 MV m^{-1} at a Q-value of 3×10^9 could be reached with a Nb_3Sn resonator at 4.2 K instead of 1.8 K, as in the case of bulk Nb resonators. However, the promise of much higher fields in Nb_3Sn cavities has not yet been proven. Thermal instabilities limit the gradient well below the fields of good Nb cavities. Inclusions of non-stoichiometric Nb_3Sn phases are thought to be the nucleation centres for a thermal instability.

4.2. High gradients

At present, Nb resonators in accelerators are operated at gradients considerably below the physical limitation of the superconductor. The main limitations are thermal instabilities (quench) and field emission. Research and development is being undertaken to explore the reason for these limits and to search for improvements. Material samples are being investigated to examine the effect of different fabrication, treatment and handling procedures. However, finally, these results must be confirmed in measurements of full size cavities under radiofrequency operations. Single-cell resonators are an appropriate test vehicle for this purpose. They allow a fast turnaround time and they sample enough surface area under realistic radiofrequency conditions. Multicell resonators with auxiliary components for accelerator application are more difficult to handle and will lag behind in performance. Nevertheless, the hope is that multicell cavities will come close to the performance of single-cell resonators.

4.2.1. High-temperature firing of cavities. The model of thermal instability predicts that higher fields can be reached at a higher thermal conductivity λ of the bulk material. The

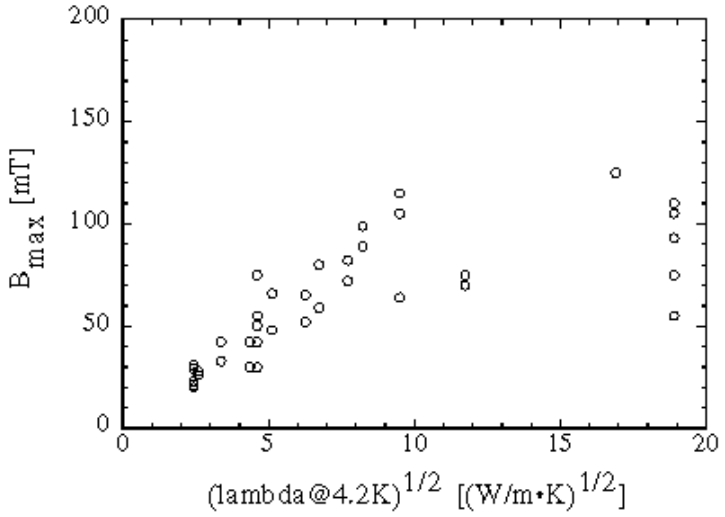

Figure 16. Measured threshold of thermal instabilities (quench) in cavities made from bulk niobium of different thermal conductivity λ [22]. For values of λ below 100 W mK^{-1} the measured maximum surface field B scales with the square root of λ, as predicted by model calculations. Above 100 mT surface field, the cavities seem to be limited by other effects than the thermal conductivity of the niobium.

quench spot can be localized by T-mapping. In most cases it was detected in the area of large magnetic field, i.e. the radiofrequency current drives the thermal instability. In figure 16 the maximum magnetic surface field of quench limited single-cell resonators is plotted against the thermal conductivity λ [22]. The data were taken from single-cell resonators at 8 GHz. The quality of the Nb was improved by induction heating the cavities at 2000 °C. The increase of thermal conductivity is due to outgassing of the Nb at such high temperatures. The benefit of higher thermal conductivity is clearly seen. This cleaning method is not practical for heavy-weight multicell resonators, because the shape of the resonator will be deformed too much. Therefore, a treatment was developed which operates at a reduced temperature [23]. The cavity is heated at 1400 °C together with titanium for about 4 h. The Ti will evaporate and cover the Nb surface. Dissolved gases like oxygen, nitrogen and carbon will be gettered by Ti so that the bulk niobium is purified by diffusion and the thermal conductivity λ is increased. With a 4 h heat treatment at 1400 °C a typical improvement factor of two has been observed experimentally. The advantage of this method is that the complete cavity is purified at a late stage of production. However, there are two major disadvantages of this cleaning method:

- the Nb is very soft after the heat treatment; the yield strength is reduced typically from 50 N mm^{-2} to around 10 N mm^{-2}, so that care is needed in handling the cavity;
- Ti will migrate into the bulk Nb, especially along grain boundaries; therefore, intensive chemical etching of the cavity is needed afterwards to eliminate additional radiofrequency losses by remaining Ti spots.

The amount of Ti diffusion can be reduced somewhat by lowering the firing temperature. However, then the processing time must be increased to compensate the reduced diffusion rate of oxygen and nitrogen. Different parameters have been tried out at Saclay with Nb samples [24]. A 1 h heating at 1350 °C for Ti evaporation and up to 20 h for diffusion process at 1250 °C seem to be a good compromise. A different method could be to separate the temperature of the evaporating Ti from that of the heated cavity. Ti wires could be heated by electric current, whereas the furnace with the cavity is kept at a lower temperature. Experiments are planned but need substantial changes of the furnace construction. It should be noted that a heat treatment of Nb at 1400 °C without titanium gettering will actually deteriorate the thermal conductivity of the niobium. The reason is that even in an UHV furnace the residual gas pressure of oxygen is so high that the oxygen will diffuse into the Nb.

The increase of the bulk thermal conductivity λ of Nb is one clear benefit of the heat treatment, but there is evidence that global material properties of the bulk niobium can be improved by the right heat treatment, too. Niobium is forged and rolled during fabrication. As a final step, the niobium sheets are recrystallized by heating around 800 °C, so that stress in the bulk is relaxed and uniform grain size is gained. Nevertheless inductive measurements of this material exhibit a transition near the upper critical field H_{c2} which is not sharp [25]. This is explained by the presence of 'pinning centres' which prevent a free movement of flux tubes in the intermediate state. Candidates for pinning are lattice distortions, inclusions of foreign material, clusters of impurities, etc. Experiments with samples concluded that temperatures of 1200 °C or higher are needed to obtain the sharp magnetic transition of a good superconductor [25]. The disappearance of pinning centres is due to a homogenization process of the bulk material during firing. Pinned flux tubes will be bent under the influence of radiofrequency field and thus produce additional losses. Therefore, homogenization of the bulk superconductor is necessary to reach high fields in radiofrequency cavities.

There is clear evidence that heat treated cavities are less sensitive to thermal instabilities. The beneficial effect of the heat treatment can be separated into:

- improving the thermal conductivity by solid-state gettering;
- homogenization of the bulk material.

It seems that the effectiveness differs between the Nb material of the various manufacturers. More systematic investigations are needed to separate the functions and to optimize the individual improvements.

4.2.2. Material investigations. It is well established that a layer of about 150 μm of Nb must be removed after cavity fabrication to reach high fields and high quality factors (= low radiofrequency loss). The so-called damaged layer contains dirt, inclusions and other impurities which will produce radiofrequency losses or initiate a quench. Figure 17 shows the quality factor and quench field of a single-cell resonator after successive material removal [26]. A low surface resistance can be reached after only 50 μm etching, whereas the quench limit still improves after 300 μm total removal rate. The radiofrequency loss of a single, small normal conducting defect will not be noticeable in the integral measurement of the quality factor but can initiate a thermal instability.

There is the suspicion that dust, dirt or other foreign material is pressed into the Nb during forging and rolling of the sheets. Obvious handling mistakes can be detected by careful visual inspection of the surface, by a discoloration at defects after anodizing the Nb sheets or by a 'rust' test (immersing the sheets into water and searching for traces of rust due to iron particles). These quality controls are essential but are only sensitive to surface defects. They cannot detect buried defects which will be uncovered after the next chemical etching process. Therefore, a scanning apparatus with an eddy current has been developed at DESY together with the National Institute for Material Research BAM (Bundesanstalt fuer Materialpruefung) [27]. The eddy current measurement is sensitive to changes of the bulk electric conductivity. Therefore, inclusions of foreign material as well as mechanical defects

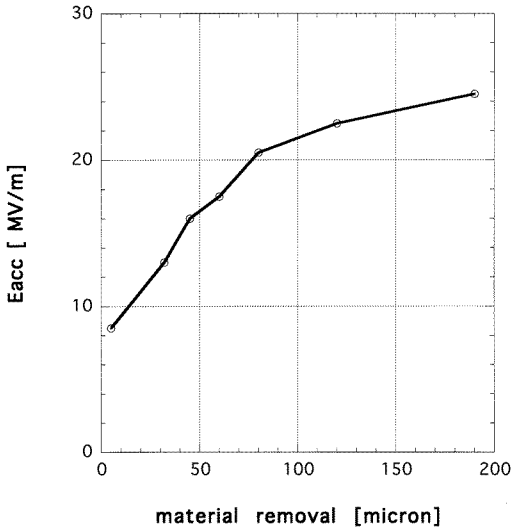

Figure 17. Increase of quench threshold by successive removal of Nb from the inner cavity surface [26]. Most likely the quench is initiated by local impurities in the bulk niobium due to contaminations during the rolling process of the Nb sheet production. A 'damage layer' of about 150 μm must be removed until a clean surface can be prepared for the superconducting surface currents.

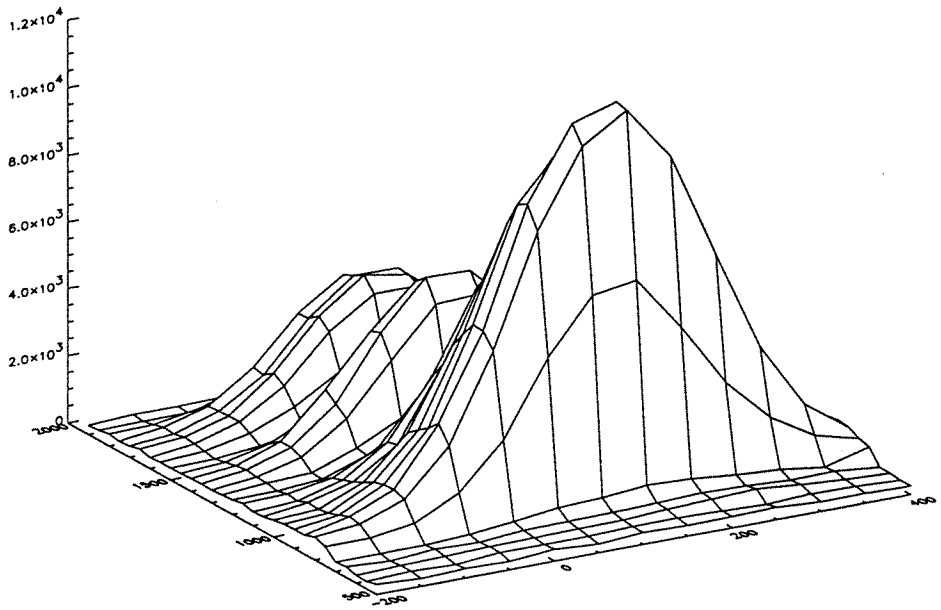

Figure 18. An example of the result of quality control on Nb sheets (280 mm × 280 mm × 2.8 mm) by eddy current scanning [27]. After localizing a defect by eddy current, the suspicious spot (50 μm × 500 μm) was further analysed by roentgen fluorescence. The figure shows the measured relative amplitude of iron concentration. Obviously, a small iron particle was rolled into the bulk Nb during the shut production. It should be noted that the iron particle was imbedded into the bulk and was not visible at the surface.

(laminations, cracks, voids in the bulk, etc) can be detected. The sampling depth depends on the frequency (200 kHz for 0.5 mm sampling depth) so that a depth profile can be gained by scanning a suspicious area with different frequencies. The eddy current measurement is used for fast quality control of the Nb sheet material before cavity fabrication and for examination of welds during the fabrication process. With a prototype of the eddy current scanning apparatus, 700 Nb sheets of the size 152 mm × 152 mm × 2.8 mm were examined. Suspicious areas were detected with inclusions of foreign material: iron, tantalum and some elements not yet identified (see figure 18). Some welds of nine-cell cavities were scanned with this apparatus, too. There is a significant correlation between untypical eddy current signals and quench locations found by temperature mapping of the superconducting cavity. In another example, a quench spot (at the sheet material, not at the weld) was localized by T-mapping and verified afterwards by eddy current. Roentgen fluorescence measurements identified the nature of the spot as a Ta cluster in the bulk Nb.

4.3. Field emission studies

Field emission (FE) is the second important limitation of the field strength in superconducting cavities. The experimental signature is the onset of x-radiation and the strong increase of additional losses in the cavity. In practical operation three handling procedures turned out to be effective in reduction of field emission.

• The final cleaning and assembly procedure should be undertaken at stringent dust free conditions.

• Continuous or pulsed operation of the cavity for some time will reduce the strength of field emission (radiofrequency conditioning). This operation is more effective if the cavity vacuum is flooded with He gas in the pressure range of 10^{-5} mbar (He processing).

• When using pulsed radiofrequency operation with high peak power (HPP), the offered radiofrequency power is considerably higher than needed to establish the cavity field at the onset of field emission. During the radiofrequency pulse very high fields and strong field emission loading is observed in the cavity. Some field emitters are 'destroyed' by this operation (see figure 22 later) so that the onset of field emission is shifted to higher cavity fields afterwards (see figure 19).

These are pragmatic means to fight field emission, but special test set-ups are needed to explore the physical nature of the field emission process. There are three different methods of investigation.

(a) Sampling a relative small surface with localized high DC electric field for field emitting spots. Clean surfaces are investigated as well as those with artificial contamination.

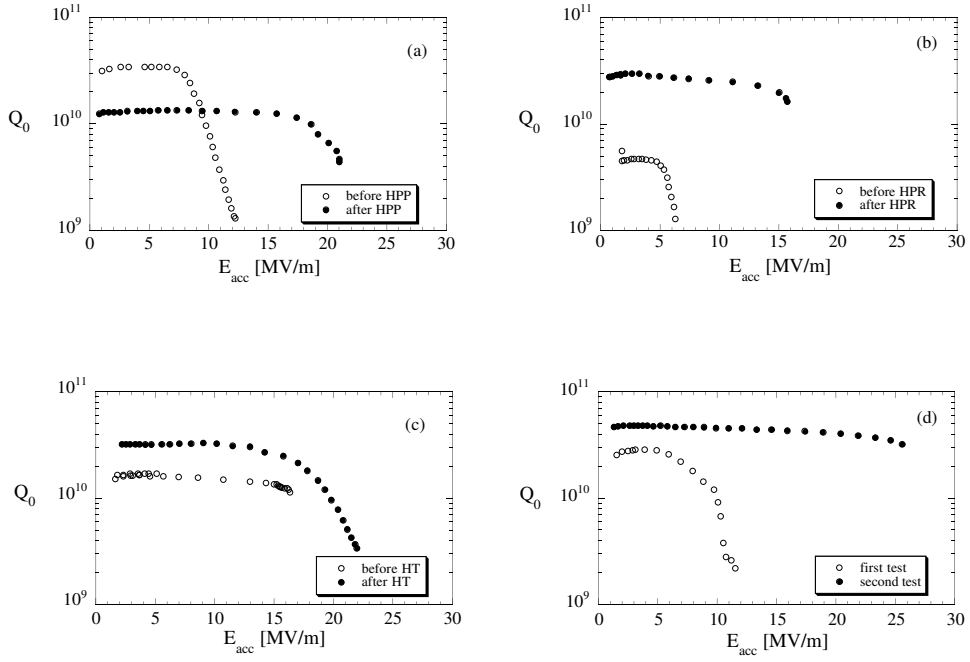

Figure 19. Examples of improved performance of superconducting cavities (1.3 GHz) after different treatments [1]. The quality factor of the cavities, Q_0, is plotted against the accelerating gradient on the beam axis. Under ideal conditions, a quality factor around 6×10^{10} is expected. (a) The cavity is heavily loaded by field emission (strong decrease of the Q_0 value); after processing with high peak radiofrequency power (HPP) the onset of field emission is shifted from 10 to 20 MV m^{-1}. (b) At first the cavity was limited by global dirt on the surface (low starting Q_0 value). Cleaning by high pressure water (HPW) improved the cavity performance. (c) Heating at 1400 °C (HT) improved the thermal conductivity and might have diluted the inclusion in the defect. The quench limit was raised from 16 to 22 MV m^{-1}, but now loading by field emission occurred. (d) At the first measurement the cavity was limited by heating at a defect (no field emission was observed). After removing a surface layer of another 50 μm by chemistry, the defect was obviously etched away.

(b) Observation and localization of field emission spots in special cavities under radiofrequency operation. After the measurement the nature of field emitters is investigated by a scanning electron microscope and the composition is analysed with appropriate techniques (energy dispersive x-ray analysis, scanning Auger, etc). For this purpose the cavity is either demountable or is cut into parts.

(c) Localize and analyse field emission in accelerator type cavities. These single- or multicell cavities have the same field configuration as accelerating structures and are handled the same way. Therefore, field emission is observed under the same operating conditions as in an accelerator but the amount of diagnostics is limited.

In a scanning DC apparatus the examined surface area is of the order of 1–2 cm^2. The DC voltage is applied between the sample Nb and a sharp needle. Therefore, localized high fields of up to 100 MV m^{-1} can be established. The field emission current is recorded during scanning of the Nb surface. The set-up of the Wuppertal apparatus is shown in figure 20 [28]. In this experiment the Nb can be heated *in situ*. An integrated scanning Auger spectrum allows investigation of the field emitting spot without breaking the vacuum. The conclusions of the investigations are:

- a fired surface (1400 °C) shows less field emission than one without heat treatment;
- a heat treatment in the temperature range 400–800 °C creates many field emitters; they can be deactivated by a succeeding high-temperature firing at 1400 °C;
- in most cases the field emitting spots are situated at irregularities (scratches, etching pits, protrusions, etc).

The reduction of field emission after firing at 1400 °C has also been observed with cavities [22]. The reason for this is not yet understood. One hypothesis is that the oxide layer of the uppermost surface is altered by the heating cycle. The reason for the activation of field emitters after the moderate heating at 400 to 800 °C is also unclear. Segregation of sulphur at grain boundaries is observed at these temperatures, but a clear correlation between sulphur content and field emission could not be verified.

At Saclay the DC field emission was investigated under complementary conditions: rather than working with the cleanest surface, it was contaminated with artificial particles [29]. As expected, field emission was found at these defects. The result can be summarized as follows:

- field emission was observed exclusively at the particles, but only a small fraction of all particles emit;
- particles with a conducting surface (iron) emit stronger than those with a dielectric oxide layer (niobium, aluminium);
- the field enhancement factor β in the Fowler–Nordheim equation (equation (19) later) can be described quantitatively by the observed geometry of the emitting particle: a round particle emits less than a sharp cornered geometry, and the geometry of protrusions can be described by a 'tip-on-a-tip' model to calculate the value of β (see figure 21).

In a second experiment at Saclay the field emission of particulates under radiofrequency condition was measured succeeding the DC investigation [29]. The Nb substrate was inserted into a special demountable resonator with high electric fields at this area. A similar tendency of high or low activity in field emission was found for the different particulates but a localization cannot be carried out in this case. At Orsay the light emitted by active field emitters was analysed in a similar resonator test set-up [29]. The measured broad spectrum indicated that thermionic emission is the origin of the light and not electro-luminescence which exhibits defined peaks. The visual observation of active field emitters gives an impressive demonstration of a processing event: after some stable glowing the particle is ejected like a burning 'comet' thus eliminating the origin of the field emitting process [29].

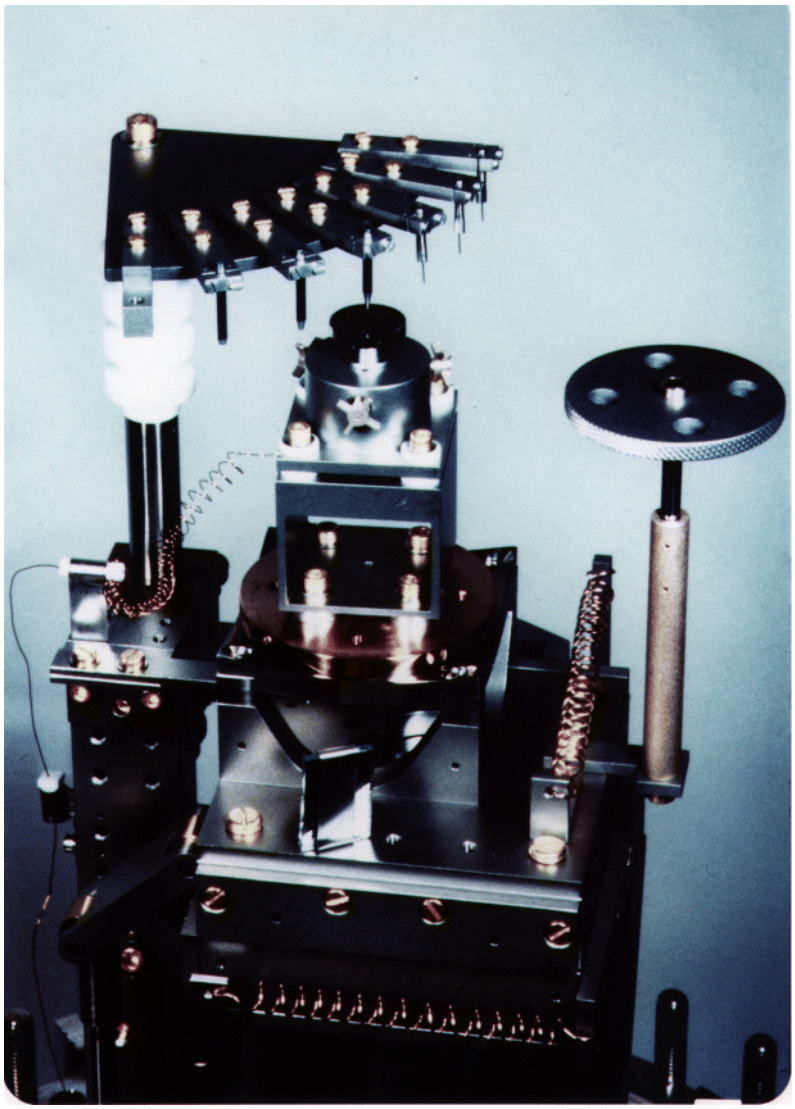

Figure 20. Scanning apparatus to explore field emission on metallic surfaces. A DC voltage is applied between the sample and a sharp needle, thus localizing the electric high-field region. The vacuum apparatus allows *in situ* heating, sputtering and surface imaging [28].

The experience with DC field emission suggests that small particles are the main origin of field emitted current and that geometric effects determine the field enhancement factor. It seems plausible that the same parameters are also important for radiofrequency field emission, but it cannot be excluded that other parameters might be relevant, too. Therefore, field emission studies under radiofrequency conditions are necessary. At Cornell many field emitters in cavities have been localized by temperature mapping. After dismounting (or

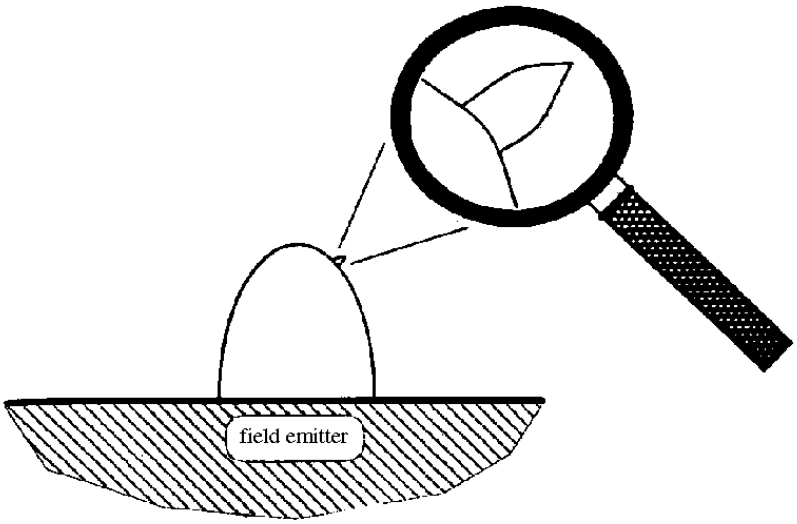

Figure 21. The field emission current is determined by the local electric field strength. This field might be enhanced by geometric effects. The measured characteristic of the field emission current can be quantitatively described by a tip-on-a-tip model: the geometric field enhancement factor of the large protrusion is multiplied by the second factor of the small tip on top [29].

cutting) the cavities, field emission sites were examined by a scanning electron microscope. Those spots which experienced high radiofrequency peak power or He processing are characterized by [22]:

- an obvious molten, crater-like left-over of material other than Nb;
- a 'star burst' like footprint around the middle crater.

The 'star burst' image is due to a different secondary electron emission coefficient as compared to the normal Nb surface. Figure 22 displays such an event. Elements like indium (from the flange sealing material) and chromium (from stainless steel parts) could be identified in the centre region. At places where field emission without processing took place, small spheres were found on top of a protrusion. The most plausible explanation is that during field emission the tip of the emitter is at melting temperature. The high temperature could be due to resistive heating by the field emitted current or to ion bombardment by a plasma. In the case of He conditioning the field emitted current will ionize the He gas. The He ions will selectively bombard the area of the emitting spot because of the local electric field enhancement. There is evidence that the extinction of an emitting spot and the 'star burst'-like signature are due to a sudden plasma discharge.

4.4. New materials

Compounds like NbN ($T_c = 17.2$ K) and (NbTi)N ($T_c \simeq 17$ K) are under investigation at several laboratories [30]. The measured residual surface resistance of these films is rather high. Furthermore, it increases with increasing radiofrequency field. The maximum magnetic surface field on small samples corresponds to accelerating gradients below 5 MV m^{-1}.

These limitations are explained by imperfections in the film morphology, which could be cured by proper substrate preparation and coating technique. However, at present, these

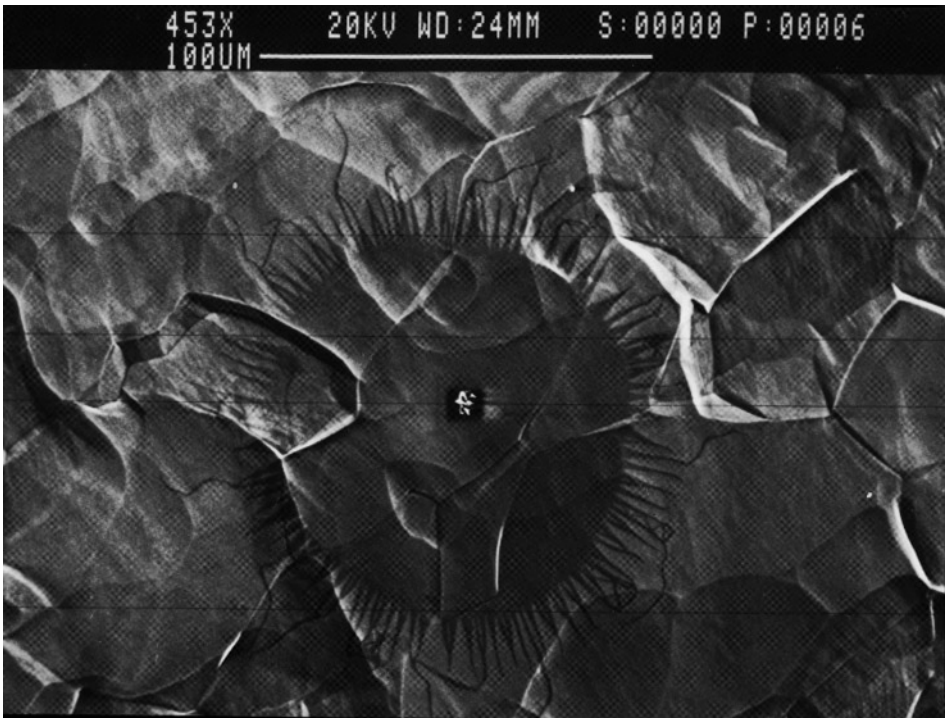

Figure 22. A 'star burst' picture of a field emitter after processing with high pulsed radiofrequency power. The location of the field emitter was determined with a temperature mapping system. After dissection of the cavity the suspicious area was examined by a scanning electron microscope [22].

materials are not applicable for accelerator technology.

High-temperature superconductors were discovered in 1980 [31]. They promise operation at the temperature of liquid nitrogen (77 K) instead of 4.2 K with liquid helium. Many different compounds (presently about 40) are being investigated, YBaCuO being the most popular one.

Many possible applications of planar microwave components have been identified which use epitaxial thin films of high-temperature superconductors [32]. Coating of cavities for accelerator application, however, results in polycrystalline and textured layers. The radiofrequency surface resistance and the maximum surface fields are determined by loss mechanisms in the grain boundaries (granular superconductor). With the present knowledge of film coating, the performance of a high-temperature superconductor is far below the needs in accelerator application.

5. General design criteria

5.1. Comparison between normal conducting (NC) and superconducting (SC) accelerating cavities

5.1.1. Power consumption. The radiofrequency power needed to establish a certain accelerating voltage is largely determined by the resistivity of the wall material. In the normal conducting case, a material with high conductivity is chosen like copper or

aluminium. The shape is optimized by 'pushing' the electric field lines near to the accelerating axis by the so-called nose cone design (see figure 13). In the superconducting case, the radiofrequency loss is reduced (i.e. the Q-value is enhanced) by typically five to six orders of magnitude. The dissipated energy has to be cooled at cryogenic temperatures. Therefore, the power consumption of the refrigerator has to be considered, too. As a rule of thumb, 1 W of refrigerator power at 4.2 K needs an AC primary power of 500 W. The refrigerator efficiency increases with the size of the installation, so the quoted number will vary by a factor of two from a very small to a very large installation. In table 3 a comparison between a normal conducting and superconducting design (500 MHz, storage ring application) is listed. One can see that the power need of a superconducting system is drastically reduced, including the cryogenic effort, of course. This is why the shape of a superconducting cavity need not be optimized for low power consumption (the so-called 'shape factor' R/Q is explained in section 7.2). There is no need for a 'nose cone' design and the iris diameter can be opened. As consequence, the coupling between the bunch fields and the cavity wall ('wake fields') is considerably reduced. The strength of the wake fields scales inversely with the third power of the iris diameter. Therefore, the deterioration of the beam quality by these wake fields is substantially reduced in the superconducting design.

5.1.2. Limitation of the accelerating gradient under continuous wave operation. In the normal conducting case, the gradient is limited by the difficulties of the remaining heat, produced by the radiofrequency losses. The order of magnitude is a maximum of 100 kW m^{-1}, which corresponds to not more than 2 MV m^{-1} accelerating gradient. In the superconducting case, the maximum gradient is limited by the critical field H_c of the superconducting material (strictly speaking by the superheated field H_{sh}, which takes into account the time structure of the radiofrequency field, H_{sh} is somewhat higher than H_c, see section 6.2). In the case of niobium, this corresponds to about $E_{acc} = 55$ MV m^{-1}. In practice, however, field emission or thermal instabilities will set a lower limit. The highest gradients that have been achieved in Nb resonators so far are 43 MV m^{-1} in single-cell and 27 MV m^{-1} in multicell structures.

5.1.3. Limitation of the accelerating gradient under pulsed conditions. Under pulsed conditions the average radiofrequency loss will be reduced according to the duty cycle. Therefore, normal conducting cavities will not be limited by cooling restrictions, if the duty cycle is small enough. Field emitted electrons will produce dark current or initiate sparking, thus limiting the maximum gradient. In superconducting cavities the maximum gradient is limited by field emission and thermal instabilities. It has been observed that for short radiofrequency pulses the onset of a thermal instability might be delayed, thus allowing a somewhat higher gradient than in continuous operation (up to 30%).

Table 3. Comparison of the power consumption between a normal (NC) and superconducting (SC) accelerating structure at 500 MHz (length 1 m, $E_{acc} = 1$ MV m^{-1}, phase velocity $\beta = 1$).

Value	SC	NC
Q	4×10^9	4×10^4
P at 4.2 K	0.7 W	
P at 300 K	0.35 kW	35 kW

5.1.4. Choice of frequency. The superconducting surface resistance grows with the square of the frequency (see equation (10) later). It can be compensated for by lowering the temperature at the additional cost of refrigerator power. However, above 5 GHz the optimum temperature is too low for technical realization. Another strong argument against high frequencies is the early onset of a global thermal instability. It is driven by the strong temperature-dependent BCS surface resistance which is dominant at high frequencies (because of the explicit ω^2 term in equation (10)). Therefore, frequencies around 1 GHz or lower are favoured for superconducting accelerating systems.

In a normal conducting cavity the surface resistance scales only with the square root of the frequency (skin effect). Therefore, the reduction of the surface area at high frequencies (cavities are smaller at higher frequencies) is dominant and results in lower radiofrequency losses.

5.2. Optimum gradient

It seems plausible that a superconducting accelerating cavity should be operated at the highest possible accelerating gradient. This is true, if the beam energy must be established in the shortest length or if a low number of cavities is crucial for the beam quality. For a large-scale accelerator complex, however, the need for a cost optimized design will determine the best accelerating gradient. For a given final energy the optimum is given at the minimum of investment or the sum of operating and investment costs. In a detailed optimization a number of parameters must be considered. However, there are two major cost items which dominate the investment cost and thus the optimization procedure: the refrigerator installation and the cavity/cryostat system.

5.2.1. Cryogenic power. The radiofrequency losses per unit length increase with the square of the gradient:

$$P/m = E_{\mathrm{acc}}^2 \left(\frac{R}{Q}\right)_m^{-1} Q_0^{-1} \tag{2}$$

where P/m is the radiofrequency loss per unit length, E_{acc} the accelerating gradient, $(R/Q)_m$ the characteristic impedance per unit length and Q_0 the quality factor of the cavity.

The total length of the accelerator scales inversely with the gradient:

$$L = \frac{U}{E_{\mathrm{acc}}} \tag{3}$$

where L is the length of the accelerator and U is the total voltage of the accelerating system.

The refrigerator power needed is the sum of the static loss, the radiofrequency cavity loss in the accelerating mode and the induced higher-order mode losses. To first order the fundamental mode cavity loss is the dominant part. Under this assumption the refrigerator power and thus the investment cost of the refrigerator will scale proportionally to the accelerating gradient:

$$C_{\mathrm{refrigerator}} \propto \left(\frac{P}{m}L\right) \propto E_{\mathrm{acc}} \tag{4}$$

where $C_{\mathrm{refrigerator}}$ is the investment cost of the refrigerator.

5.2.2. Cavity costs. There are linear costs which scale with the total length of the accelerator and thus inversely with the accelerating gradient for a given total accelerating voltage. In the case of a superconducting radiofrequency system, the dominant linear costs are the cavities and the cryostats themselves:

$$C_{\mathrm{cav}} \propto E_{\mathrm{acc}}^{-1} \tag{5}$$

where C_{cav} is the investment cost of cavity and cryostat.

Under these simplified assumptions, the total investment cost is given by the sum of refrigerator and cavity costs:

$$C_{\mathrm{total}} = C_{\mathrm{refrigerator}} + C_{\mathrm{cav}} = a_{\mathrm{refrigerator}} E_{\mathrm{acc}} + \frac{a_{\mathrm{cav}}}{E_{\mathrm{acc}}} \tag{6}$$

where C_{total} is the total investment cost, $a_{\mathrm{refrigerator}}$ the cost calibration for the refrigerator and a_{cav} the cost calibration for the cavities and cryostats.

The total costs are dominated by the cavity costs at low gradient E_{acc}, whereas the refrigerator costs dominate at high gradient. The minimum of total costs is reached, when cavity and refrigerator costs are equal. Two examples are given to demonstrate the absolute value of the best gradient.

(a) The superconducting radiofrequency installation in the HERA storage ring: the cavity/cryostat costs are around 400 TDM per active accelerating metre. The high costs are mainly due to the many warm/cold transitions (only two cavities per cryostat), the external cryogenic distribution system (one valve box per cryostat) and the complicated fabrication sequence of the cavities themselves (many welds in an electron beam welder). Figure 23 shows that the cost minimum is around an E_{acc} of 8 MV m^{-1}.

(b) The example of a linear accelerator with pulsed operation (TESLA [1]): it is assumed that the linac is operated during 1.3 ms at a repetition rate of 5 Hz. Therefore, the refrigerator load is reduced to 0.65% as compared to a continuous operation, like a storage ring. In this example, the linear costs are estimated to be 80 TDM per metre. It is the hope that this low number can be reached by a cryostat design with long cold sections, an integrated helium distribution (see figures 10 and 11) and by simplified cavity production techniques (like hydroforming). The broad minimum extends from 40 to 80 MV m^{-1} (see figure 24). The shift of the optimum gradient to higher values is mainly due to the pulsed operation, thus reducing the refrigerator load.

5.3. Optimum temperature

In most applications the cryogenic temperature is either near to 4.2 K or 1.8 K. The advantage of 4.2 K is that this is the temperature of boiling helium at atmospheric pressure. Therefore, sub-atmospheric conditions can be avoided so that there is no risk of contaminating the helium circuitry with air. Furthermore, the refrigerator components (warm compressor, cold turbines or expansion engines) are well developed. Unfortunately, the operating temperature of superconducting resonators must be lower if the resonator frequency is in the GHz regime. The reason is the scaling of the BCS surface resistance with frequency and temperature (see also equation (10)):

$$R_{\mathrm{BCS}} \propto f^2 \exp\left(-\frac{\Delta}{kT}\right) \tag{7}$$

where R_{BCS} is the BCS surface resistance, f the frequency, T the temperature, Δ the energy gap and k the Boltzmann constant.

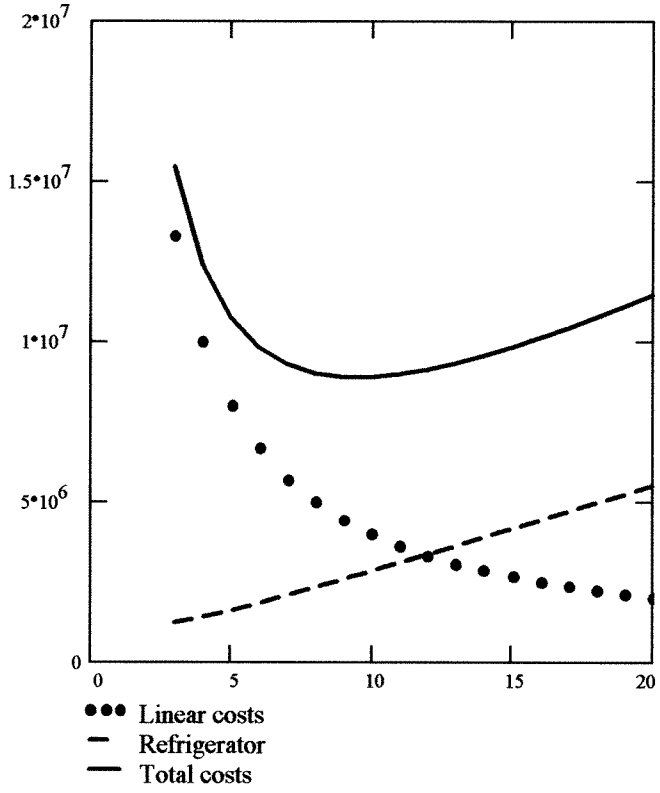

Figure 23. Cost optimum of a superconducting accelerating system for continuous wave operation (e.g. in a storage ring). There are two main contributions to the investment costs: linear costs (cavities, cryostats) and refrigerator costs. For a fixed total voltage they scale with E_{acc}^{-1} and E_{acc}, respectively (see equation (6)). The cost minimum is given when both contributions are equal.

At frequencies above 1 GHz the BCS surface resistance at 4.2 K is so high that the gradient in the cavity will be limited by global thermal heating. The BCS surface resistance can be lowered by reducing the operating temperature. The liquid helium will become superfluid below the λ point at 2.2 K. A quench limited superconducting cavity will reach higher fields if operated below the λ point. Therefore, 1.8 K is chosen in most cases as the operating temperature for cavities in this frequency range to have some safety margin against crossing the λ point.

The choice of the operating temperature of 4.2 K below 1 GHz and 1.8 K for higher frequencies is a pragmatic conclusion for reasons given above. If the investment and operating costs of the refrigerator system are to be minimized, a more detailed optimization is needed. The total cryogenic power P_{total} is given by

$$P_{\mathrm{total}} = P_{\mathrm{static}} + P_{\mathrm{RF}} = P_{\mathrm{static}} + P_{\mathrm{BCS}} + P_{\mathrm{residual}} \tag{8}$$

where P_{total} is the total cryogenic loss, P_{static} the static losses, P_{RF} the losses by radiofrequency, P_{BCS} the radiofrequency losses by BCS surface resistance and P_{residual} the radiofrequency losses by residual surface resistance.

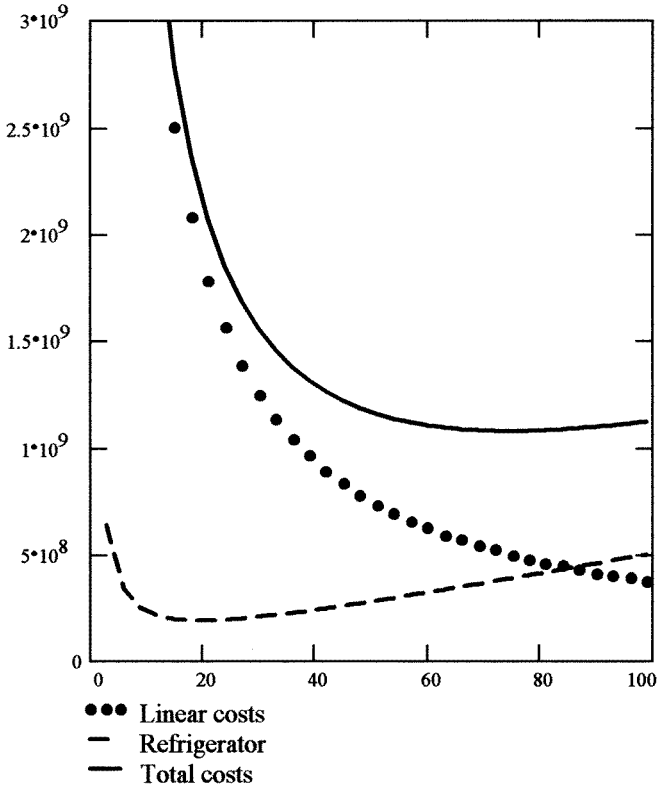

Figure 24. Cost optimum of a superconducting accelerating system for pulsed operation (TESLA proposal). The RF duty cycle of 10^{-2} reduces the cryogenic load; therefore, the cost minimum of investment cost is shifted to higher accelerating gradients (compare with figure 23 for continuous wave application).

The AC compressor power P_{AC} to produce refrigeration power P_{total} is given by

$$P_{\mathrm{AC}} = P_{\mathrm{total}} \frac{300 - T}{T} \frac{1}{\text{efficiency}} \tag{9}$$

where P_{AC} is the AC compressor power of a refrigerator, efficiency is the efficiency of the refrigerator system and T the temperature (K).

The minimum of the compressor power P_{AC} determines the optimum temperature. Details of the calculation depend on the chosen cavity geometry, frequency and the value of the absolute refrigerator power (the efficiency depends on the size of the refrigerator). Accelerating structures for $\beta = 1$ application are analysed in [33]. In figure 25 the capital costs are plotted against temperature. The parameters are a gradient of 10 MV m^{-1} and a residual quality factor of 6×10^9. The chosen frequencies represent storage ring (350 MHz, CERN; 500 MHz, DESY) and linac applications. At 350 MHz there is a broad minimum around 4.2 K, whereas at 500 MHz the optimum is near to 3 K. However, the advantage is not so high to risk sub-atmospheric operation. Around 1 GHz the choice of 1.8 K seems right, whereas at 3 GHz one should even use a lower temperature.

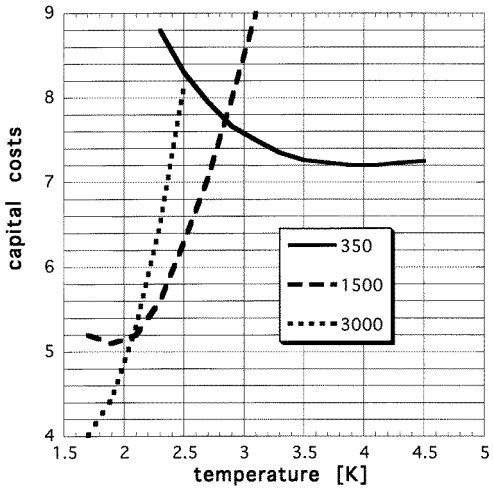

Figure 25. Optimum temperature in order to minimize the investment costs of the refrigerator installation. Design parameters are continuous operation at $E_{acc} = 10$ MV m^{-1} and a quality factor of 6×10^9 of the superconducting cavity. Parameters are the operating frequency in MHz. The superconducting loss scales with the square of the frequency but is lower at lower temperatures (see equation (10)).

6. Fundamentals of RF superconductivity

6.1. Surface resistance

It is well known that in the superconducting state a DC current will not dissipate heat. Therefore, superconducting magnets require cooling power only for losses from heat conduction or radiation from the warm part to the cold mass. In the case of alternating current (even more for high-frequency applications) there is loss in the superconducting state. This is predicted by the BCS theory of superconductivity [34]. In the normal conducting state radiofrequency current flows in a thin surface layer given by the so-called skin depth. This skin depth depends on the conductivity of the material and on the operating frequency. Typical values are 1 μm for copper at 1 GHz. In the superconducting state radiofrequency current flows in a much thinner layer as described by the 'London penetration depth'. It depends on material parameters but not on frequency. The order of magnitude is around some hundreds of angströms.

The radiofrequency loss is described by a surface resistance because it does not depend on the thickness of the bulk material. The surface resistance in the superconducting state can be calculated by the BCS theory. For temperatures below half of the critical temperature T_c it is given by the following term:

$$R_{BCS} = A\frac{1}{T}\omega^2 \exp\left(-\frac{\Delta(T)}{kT}\right) \qquad T \leqslant \frac{T_c}{2} \tag{10}$$

where R_{BCS} is the surface resistance in the superconducting state, given by BCS theory, A is a material parameter, T is the temperature in K, $\omega = 2\pi f$, where f is the frequency, $\Delta(T)$ is the energy gap of the superconducting material, k the Boltzmann constant and T_c the critical temperature of a superconductor.

The following should be noticed:

- the surface resistance drops exponentially with decreasing temperature;

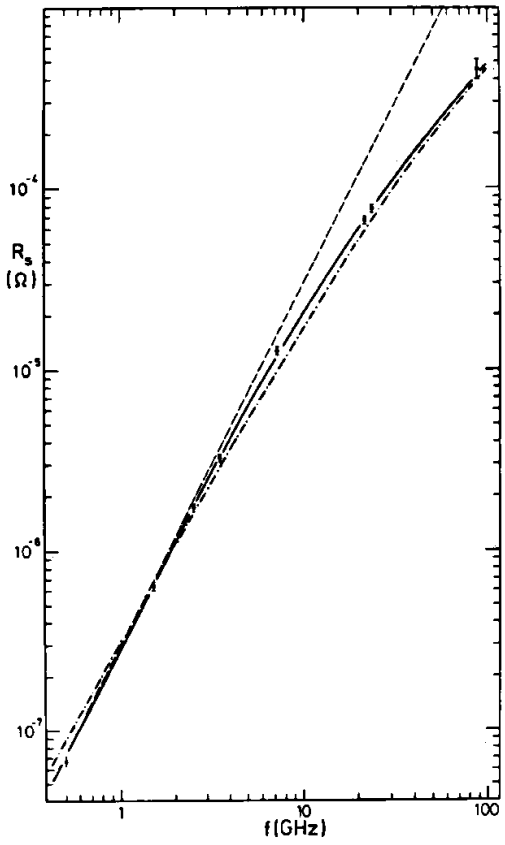

Figure 26. Measured surface resistance R_{BCS} of niobium at different frequencies at 4.2 K. The dashed curve has a slope according to a ω^2 dependency of the surface resistance (see equation (10)). There is some discrepancy between the measured data (full curve) and this curve at very high frequencies. This has been explained by a correction term. It takes into account the consequences of an anisotropy of the crystal lattice (dot-dashed curve) [42].

• the surface resistance increases with the square of the frequency.

Figure 26 summarizes measurements of the surface resistance at different frequencies for Nb resonators operated at 4.2 K.

It is an experimental finding that at very low temperatures the measured surface resistance in the superconducting state no longer decreases but approaches a constant value. Therefore, the measured surface resistance R_S is described by

$$R_S = R_{BCS} + R_{res} \tag{11}$$

where R_{res} is the residual surface resistance. Figure 27 shows a plot of the measured surface resistance of Nb_3S_n [35]. The sharp drop at the critical temperature of $T_c = 18$ K marks the transition from the normal to the superconducting state. For temperatures below 4 K the residual resistance of 2×10^{-7} Ω dominates the surface resistance. The full line represents the BCS surface resistance in the temperature range below $T_c/2$. It is calculated from the measured data by subtracting the residual resistance from the surface resistance.

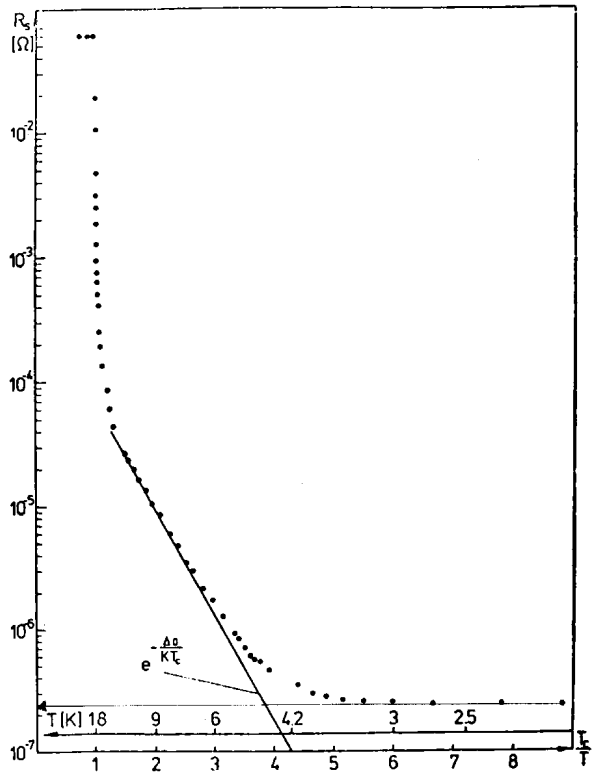

Figure 27. Measured surface resistance R_S of Nb_3Sn as a function of temperature (horizontal axis T_c/T) [35]. The sharp drop at 18 K indicates the transition to the superconducting state. Below 9 K ($= T_c/2$) the exponential dependency of R_S against 1/T gives a measure of the normalized energy gap Δ_0/kT_c (see equation (12)). At very low temperatures the surface resistance is dominated by the residual resistance.

The exponential temperature dependence of the BCS surface resistance can be written as

$$\exp\left(-\frac{\Delta(T)}{kT}\right) \overset{T<T_c/2}{\simeq} \exp\left(-\frac{\Delta(0)}{kT}\right) = \exp\left(-\frac{\Delta(0)}{kT_c}\frac{T_c}{T}\right) \tag{12}$$

where $\Delta(0)$ is the energy gap at $T = 0$ and $\Delta(0)/kT_c$ is the normalized energy gap.

The normalized energy gap is an important parameter used to describe the nature of a superconducting material. According to BCS theory its value is equal to 1.76. This value might be larger (or smaller) in the case of a strong (weak) coupling superconductor. For example, the value of the normalized energy gap is 1.83 for Nb whereas it is 1.93 for Nb_3S_n as representative for a strong coupling superconductor. The temperature-dependent measurement of the surface resistance is a direct way to determine the value of the normalized energy gap. It was in fact such a cavity measurement which clearly concluded the strong coupling nature of Nb_3S_n for the first time [35].

6.2. Critical field

Under ideal conditions there is no magnetic field inside the superconductor (Meissner–Ochsenfeld effect). There are two experimental ways to reach this state.

- The material is cooled below the critical temperature and then the external magnetic field is raised. Under these conditions, the displacement of the magnetic field could be explained just by shielding currents. They are induced by the time-varying magnetic field when being switched on and will flow in the 'ideal conductor' without loss. The external magnetic field is compensated according to the 'Lentz' law.
- The external magnetic field was applied before cooling below the critical temperature. Because there is no induction in the superconducting state, a material with zero resistance cannot expel the external field. However, it is the finding of the Meissner–Ochsenfeld experiment that the external magnetic field is expelled as well. This experiment demonstrates that a 'superconductor' cannot be explained by zero resistivity alone, but that superconductivity is a new phase of the material.

The superconducting state will be destroyed by an external magnetic field above the so-called critical value H_c. The value depends on the material and the temperature:

$$H_c(T) = H_c(0)\left(1 - \left(\frac{T}{T_c}\right)^2\right) \tag{13}$$

where $H_c(T)$ is the temperature-dependent critical field, $H_c(0)$ the critical field (at $T = 0$) of the superconductor, T the temperature and T_c the critical temperature of the superconductor.

There are two classes of superconductors which differ in the behaviour at the critical field. In type I superconductors, the superconductivity brakes down sharply at H_c. In type II superconductors, there exists a transition region between H_{c1} and H_{c2} ('Shubnikov phase'): the magnetic field starts to penetrate the bulk above H_{c1} in the form of small flux tubes ('fluxoids') with a normal conducting core. The magnetic flux inside the fluxoids equals the value of H_{c2}. The remaining bulk stays in the superconducting state. The number of fluxoids increases for increasing external magnetic field. At an external magnetic field of H_{c2}, the whole bulk material is penetrated by fluxoids, so that the material has lost its superconducting property. The thermodynamic critical field H_c is about the geometric mean of H_{c1} and H_{c2}:

$$H_c = (H_{c1}H_{c2})^{1/2} \tag{14}$$

where H_c is the thermodynamic critical field (type I, II superconductor) and H_{c1}, H_{c2} is the lower and upper critical field (type II superconductor).

The above-mentioned critical fields are defined for static magnetic fields. In the case of radiofrequency application it is decisive whether the phase transition from superconducting to the normal conducting state is faster or slower than the radiofrequency period. For type I superconductors (e.g. lead), radiofrequency fields up to H_c have been reached. Niobium is the most commonly used type II superconductor. A maximum surface magnetic field of 170 mT has been reached in a Nb resonator. This is near to $\mu_0 H_{c1}(0) = 180$ mT of very clean niobium, but lower than $\mu_0 H_c(0) = 200$ mT. It is believed that H_{c1} presents no fundamental limit for radiofrequency fields. Furthermore, it is predicted that due to the fast varying radiofrequency field the phase transition is shifted to a value above H_c, the so-called superheated field H_{sh}. In the case of niobium, $\mu_0 H_{sh}(0)$ is calculated to be 240 mT [36].

Table 4. Properties of some superconducting materials used for radiofrequency application (T_c, critical temperature; $H_c(0)$, critical magnetic field at 0 K; $H_{sh}(0)$, superheated field at 0 K; max E_{acc}, accelerating gradient at H_{sh}, assuming a ratio of 4.2 mT per 1 MV m^{-1} accelerating gradient).

Superconductor	T_c (K)	$\mu_0 H_c(0)$ (mT)	$\mu_0 H_{sh}(0)$ (mT)	max E_{acc} (MV m^{-1})
Pb	7.2	80	105	25
Nb	9.2	200	240	57
Nb_3Sn	18.2	540	400	95

6.3. Experimental limitations of the surface resistance

The superconducting surface resistance R_S consists of two parts:

$$R_S = R_{BCS} + R_{res} \tag{15}$$

where R_S is the surface resistance, R_{BCS} the BCS surface resistance and R_{res} the residual surface resistance.

One should note that the BCS surface resistance depends on frequency and temperature. It will be higher at higher frequencies and higher temperatures (see equation (10)). The dependency on material properties like mean free path of electrons or normal-state resistivity is contained in the parameter A in equation (10). The residual resistance determines the lower limit of the measured surface resistance. The reason for a high value of the residual resistance may be trivial: dirt on the surface or normal conducting particles in the bulk but penetrating the surface. This can be avoided by purification of the material and by adequate cleaning (e.g. high pressure water, ultrasonic) and handling (clean room conditions) methods. Two definite effects are known to contribute to the value of the residual surface resistance:

- loss due to frozen static magnetic field;
- loss due to hydrogen in the bulk niobium ('hydrogen disease').

6.3.1. Loss due to trapped magnetic field. According to the Meissner effect a static magnetic field is expelled from a superconductor. In a type II superconductor (e.g. niobium) magnetic flux will penetrate the bulk at external fields between H_{c1} and H_{c2}. Values from 130 to 180 mT have been measured for niobium, depending on the purity and quality of the metal. Therefore, one would assume that the earth magnetic field of only 0.03 mT would not affect the properties of a superconducting cavity. In practice, however, one has to shield the cavity against the earth magnetic field during cool down to reach quality factors well above 10^9. The 'magnetic' loss is caused by the normal conducting core of the flux lines. Measurements on Pb (type I superconductor) and niobium (type II superconductor) samples clearly conclude that 100% of the earth magnetic flux is trapped in the bulk during cool down [37]. The measured residual resistance R_m could be parametrized by:

$$R_m = R_n \frac{H_{ext}}{H_{c2}} \tag{16}$$

where R_m is the residual resistance due to magnetic field, R_n the normal conducting surface resistance of the material, H_{ext} the external magnetic field and H_{c2} the upper critical field of the superconductor.

It is worth noting the following points.

• The earth magnetic field (in the order of 0.03 mT) is *not* expelled during the superconducting phase transition of Nb and Pb. In this sense, there is no Meissner effect at this field level. The reason for this phenomenon is not understood. It is argued that temperature gradients in the bulk during cool down could create normal conducting islands within the superconducting surrounding. Magnetic flux in these islands cannot escape, even after a complete phase transition. A non-uniform distribution of the critical temperature T_c in the bulk (by inhomogeneities) will have the same consequence.

• Nb sputtered Cu cavities seem to be insensitive to 'magnetic' losses. The reason is that H_{c2} of a sputtered Nb film is much higher than that of bulk Nb (so that the equivalent residual resistance is much lower (see equation (16)).

6.3.2. Loss due to hydrogen ('hydrogen disease'). Some years ago a peculiar loss mechanism was observed. Cavities showed enhanced losses, depending on cool down conditions. The first observations were performed at accelerator installations, whereas laboratory measurements in vertical cryostats seemed not to be affected. After intensive investigations at several laboratories the effect could be identified as segregation of niobium hydride on the surface [38]. Hydrogen is dissolved in the bulk niobium and has a high mobility at room temperature. Around 100 K the hydrogen will segregate as niobium hydride. Its lattice constant is larger than that of niobium, and therefore it will segregate preferable at dislocations or on the surface. Niobium hydride is a normal conductor and thus will produce radiofrequency losses. If a niobium cavity stays for some time (several hours) at a temperature around 100 K, niobium hydride will be formed preferably at the surface because the mobility of hydrogen is still high enough in order to diffuse to the surface. In the case of a fast cool down to 4 K the amount of niobium hydride on the surface will be small. After warm up to room temperature, the niobium hydride is dissolved again.

It is known that atomic hydrogen is produced during electro-polishing, so that the hydrogen content in the bulk niobium will be considerably enhanced after this cleaning procedure. Less intensive loading of niobium with hydrogen was measured after chemical polishing. A heating of the niobium at 800 °C under vacuum will effectively 'de-gas' the bulk niobium from hydrogen and thus avoid the radiofrequency loss of the 'hydrogen disease'. Under certain conditions, it might not be possible to heat the complete niobium resonator at 800 °C (e.g. after brazed parts have been welded to the resonator). Here a fast cool down is the only remedy against the 'hydrogen disease'.

6.4. Experimental limitations of the accelerating gradient

6.4.1. Thermal instability (quench). One typical limitation of the maximum field in a superconducting cavity is thermal instability. The name quench is commonly used to describe the breakdown of superconductivity in magnets. Here a critical value of the magnetic field is surpassed. In radiofrequency cavities, however, the critical temperature T_c is reached by a heating process. Therefore, the name 'thermal instability' is appropriate. Nevertheless, the phrase 'quench' is often used when describing a breakdown in cavities. The experimental observation of a thermal instability is as follows.

The cavity is operated with constant radiofrequency power. At the end of the filling process an equilibrium condition is reached. The stored energy in the cavity stabilizes to such a value that the superconducting radiofrequency loss equals the transferred generator power. Above a critical value the stored energy decays to nearly zero in a short time, much faster than the time constant of the superconducting cavity. Diagnostic measurements with temperature sensors at the outer cavity wall have clearly indicated that some parts of the

cavity exceed the critical temperature of the superconductor. Therefore, it is assumed that the cavity becomes partially normal conducting, the radiofrequency dissipation is dramatically enhanced and the stored energy is decreased accordingly.

The breakdown of radiofrequency superconductivity is explained by a model of thermal instability [22]. The BCS part of the superconducting surface resistance has an exponential dependency on temperature (see also equation (10)):

$$R_{\mathrm{BCS}} \propto \exp\left(-\frac{\Delta}{kT}\right) \tag{17}$$

where R_{BCS} is the superconducting surface resistance, Δ the energy gap, k the Boltzmann constant and T the temperature.

Under steady-state conditions the temperature at the inner cavity surface is enhanced by ΔT as compared to that of the liquid helium at the outer cavity wall:

$$\Delta T = q\left(\frac{d}{\lambda} + R_k\right) \tag{18}$$

where ΔT is the temperature difference between the inner cavity surface and the liquid helium, q is the heat flux, d the thickness of the cavity wall, R_k the thermal resistance between the outer cavity wall and the cooling helium (Kapitza resistance) and λ the thermal conductivity of the cavity wall.

It is assumed that there is a small normal conducting spot (defect) on the inner cavity surface. It will produce loss according to Ohm's laws and thus raise the heat flux. Hereby the temperature of the inner cavity surface increases and finally results in an enhanced BCS surface resistance.

There is a critical value of the heat flux at which a thermal runaway is launched (because of the exponential increase of the surface resistance with temperature, see (17)) and large parts of the cavity surface will be driven to normal conductivity.

Analytic models as well as numerical simulations can describe such an avalanche effect. Parametres of the calculations are the thermal conductivity of the superconductor, the size and resistance of the normal conducting spot and the Kapitza resistance. The thermal conductivity as well as the Kapitza resistance can be measured, whereas the size and the resistance of the normal conductor are fit parameters. Figure 28 shows the result of such a simulation for Nb resonators at 1.3 GHz.

There have been many attempts to identify the defect at the localized area by careful inspection of the inner surface, sometimes after cutting the cavity. Examples of drying spots, fibres from tissues, foreign welding inclusions, welding balls (with small contact surface for conduction cooling) and cracks in the weld have been identified. In most cases the search was not conclusive, however. On the other hand, the predicted diameter of a normal conductor is in the range of 50 μm to initiate a thermal instability at a gradient of 25 MV m^{-1}.

There are two obvious ways to reduce the probability of a thermal instability:

- avoiding the normal conducting defect by extreme care in preparing and cleaning the cavity surface;
- increase of the thermal conductivity of the superconducting material.

Progress has been achieved in both areas over the last ten years. Field levels above 20 MV m^{-1} in multicell resonators and best values around 40 MV m^{-1} in single cells have been demonstrated. This is about a factor of two increase over the last decade.

6.4.2. Field emission. Field emission is the second typical limitation in high-gradient superconducting cavities. The experimental observation is as follows:

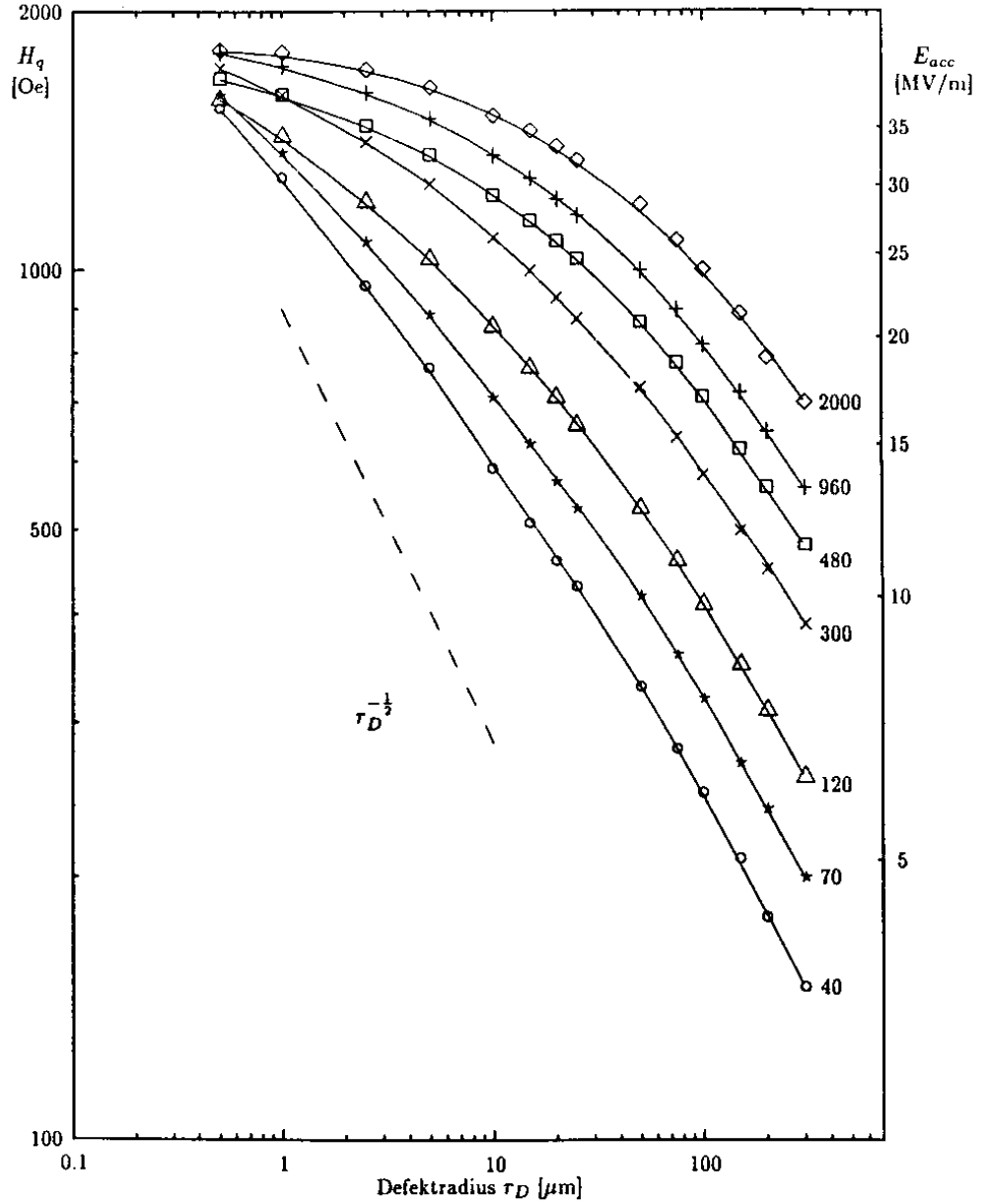

Figure 28. Model calculation of the critical surface magnetic field (thermal instability) in a superconducting resonator against the defect radius. The parameter is the thermal conductivity λ of Nb, described by the RRR value (residual resistance ratio; RRR $\simeq 4\lambda_{4.2\,\mathrm{K}}$). At the defect a normal conducting surface resistance of Nb is assumed.

- the quality factor Q drops (the radiofrequency loss grows) with increasing slope for increasing field levels;
- γ-radiation is observed outside the cryostat;
- finally the maximum field is limited by too high radiofrequency power dissipation (low Q); sometimes also a thermal instability is observed.

Figure 29 shows a measurement of a cavity which is limited by field emission. At low field the cavity exhibits a constant and high-quality factor. At the onset of field emission the quality factor drops with increasing slope when further raising the field. Finally, the gradient is limited by excessive radiofrequency power demand.

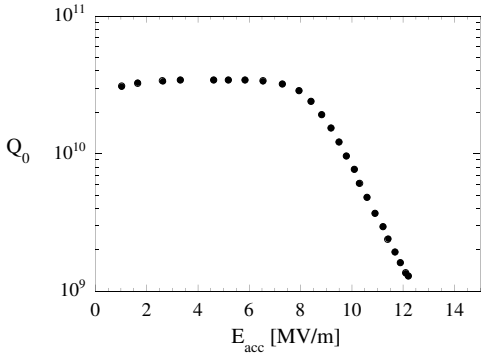

Figure 29. Typical performance of a superconducting cavity limited by field emission. At low fields the cavity experiences a high and constant quality factor. At the onset of field emission the quality factor drops and γ-radiation is observed outside the cryostat. Finally, the maximum field is limited by excessive demand of radiofrequency power.

The observation of γ-radiation is a clear indication for electrons which are accelerated by the radiofrequency field and produce γ-radiation when impacting the wall of the resonator. The appearance of an electron current has been confirmed by direct measurement with small coaxial antennas. The field emitted electrons may lead to a 'dark current' because it might show up in an accelerator with active accelerating cavities but with the electron gun switched off.

The origin of this current is the injection of electrons by field emission. It is a tunnelling effect and can be described by the Fowler–Nordheim equation [39]:

$$j_{\mathrm{FE}} = c_1 E_{\mathrm{s}}^{2.5} \exp\left(-\frac{c_2}{\beta E_{\mathrm{s}}}\right) \tag{19}$$

where j_{FE} is the electron current density, E_{s} the local electric surface field, β the field enhancement factor and c_1, c_2 are constants.

The term $E^{2.5}$ in equation (19) describes field emission in radiofrequency application whereas E^2 appears in the well known DC case. Field emission in resonators is observed for electric surface fields in the range of some 10 MV m^{-1}, whereas Fowler–Nordheim field emission from a flat surface is expected at much higher fields ($\sim$GV m^{-1}) [39]. Therefore, the field enhancement factor β is a fit factor to describe a locally enhanced surface electric field (βE_{s}). In the case of field emission from a protrusion it can be understood as the local enhancement of the electric field by the geometric effect.

There is experimental evidence that small particles on the cavity surface (e.g. dust) play an important role in initiating field emission (see section 4.3). Therefore, careful cleaning of the cavity surface is the most important remedy against field emission. However, other surface conditions, like cryo absorption of gases, determine the field emission process and need adequate care. Superconducting cavities in an accelerator should not be operated above the onset of field emission. The first reason is to avoid the additional heat by impacting electrons. The second is that dark current will spoil the reading of beam monitors and might actually deteriorate the beam quality.

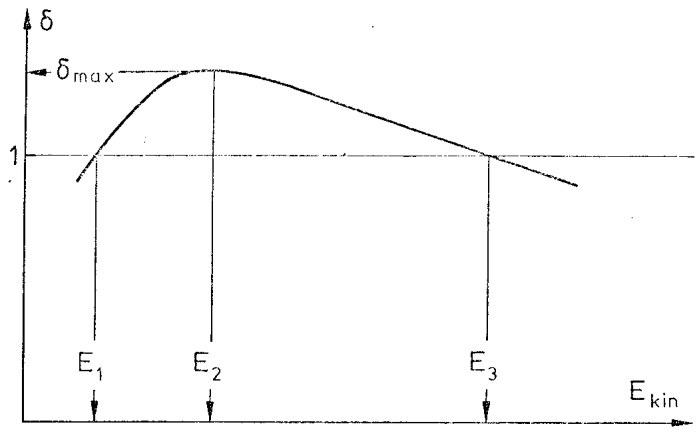

Figure 30. The primary electron might produce more than one secondary electron when impacting on a metal surface. A typical curve of the so-called secondary yield δ as a function of the input energy of the primary electron is shown in the graph. Between E_1 and E_3 (typically 50 eV and 1500 eV, respectively) the secondary yield is larger than 1. The magnitude of δ depends on material and surface conditions. Dirt and condensed gases will dramatically enhance δ up to values of about 3.

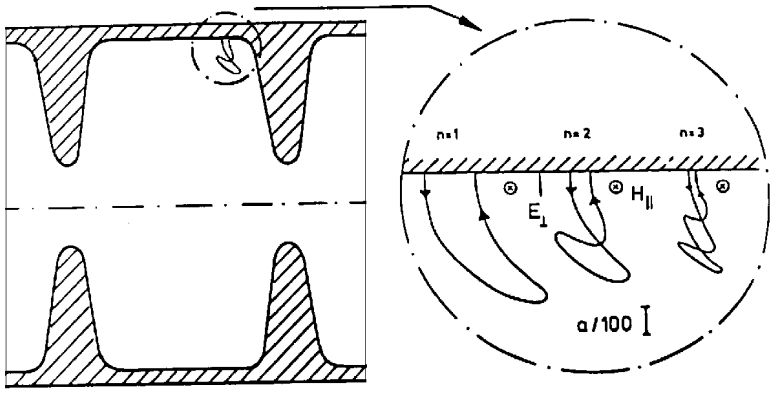

Figure 31. Cross section of a cavity which suffers from multipacting current [40]. The so-called 'one-point' trajectories start and hit the same surface. They are determined by a strong magnetic field (bending) and small electric field (energy gain). N is the number of radiofrequency periods for one closed trajectory (= order of multipacting), a is the radius of the cavity.

6.4.3. Multipacting. Multipacting (*multi*ple im*pact* electron amplification) is observed in radiofrequency components which are operated under vacuum. It is a phenomenon of resonant multiplication of electrons under the influence of radiofrequency fields. Secondary electrons can be created by a primary electron impinging on a metal surface. The secondary yield δ counts the number of secondary electrons per incident electron. The yield number δ is larger than 1 for most metals at an impact energy of the primary electron in the range

100–1000 eV. It is usually enhanced for any 'not clean' surface condition. Figure 30 shows a typical yield curve for metal surfaces.

The secondary electron will be accelerated by the electric component of the radiofrequency field and will hit the surface elsewhere. If the time for the trajectory is synchronous with the radiofrequency period and if the impact energy is in the range of $\delta > 1$, an avalanche of electrons can be created. The synchronous condition depends on details of the geometry and on the local electric and magnetic field values. Multipacting can be predicted analytically only for simple geometries. Resonant trajectories can be searched for with iterative numerical methods. This has been successfully applied for two-dimensional problems but it is still a challenge for three-dimensional radiofrequency contours.

The experimental signature of multipacting is as follows.

- There is a threshold of the field strength in the radiofrequency component. Above this threshold the radiofrequency power can be raised but it has no effect on the stored energy.
- The threshold is of sharp nature. The component can be operated below without any sign of unusual behaviour.
- The likelihood of multipacting differs for different metals and surface conditions.
- Eventually multipacting can be overcome by conditioning. This means that the component behaves normally again after being operated for some time under conditions of multipacting.
- Sometimes sparking is observed when operating in the multipacting regime and damage of the component might thereby result.

In the early development stages, superconducting cavities were plagued by multipacting. The characteristics of these trajectories were uncovered once the location of multipacting was detected by temperature mapping. The heat pulses of the multipacting current appeared at the outer cylindrical cavity wall. At this location there is high magnetic but only small perpendicular electric field. The resonant condition is determined by the bending force of the radiofrequency magnetic component. The trajectories start and end on the same surface (one-point multipacting) (see figure 31). A small electric component is essential to start the electrons and follow the trajectory. The most successful remedy against this one-point multipacting is the change of the cavity cross section from a cylindrical to a spherical shape. The magnetic resonance is destroyed by the presence of the strong electric surface field in the spherical shape [40].

6.5. Diagnostic methods for superconducting cavities

6.5.1. Temperature mapping. The most important diagnostic tool in analysing the behaviour of a superconducting cavity is the temperature mapping system. Temperature sensors are placed at the outer wall of the cavity and register the temperature distribution. From these data, information about the location and physical nature of spots with enhanced losses can be gained, such as: the location of quenches or field emissions, the scaling of losses with the cavity field, the time development of defects or the creation and processing of loss mechanisms.

Carbon resistors have proved to be sensitive and cheap temperature sensors. They are selected to have maximum sensitivity at the operating temperature. Nominal 50 Ω resistors are widely used for the temperature range from 4.2 K to 1.8 K. The outer plastic housing of the resistor might be ground off to reach good thermal contact between the cavity wall and the sensitive carbon layer. There are two different arrangements in operation.

- Fixed temperature mapping. A large number of resistors (typically more than 500) is mounted on assembly boards which are attached to the cavity. The resistors are pressed

by a spring against the outer cavity wall, the typical distance between adjacent resistors is 10 mm. The thermal contact is improved by using grease with good heat conductivity between resistor and cavity wall. The sensitivity is high enough to measure the heat produced by the BCS surface resistance. Therefore, any additional heat source (field emitting spots, impinging field emitted electrons, normal conducting defects, etc) will be localized. Moreover, the time development of a heat source can be analysed. The disadvantage of this arrangement is that a high number of sensors has to be assembled and cabled. Therefore, it is restricted to single-cell application or to only restricted surface areas of a multicell cavity.

- Rotating temperature mapping (see figure 32). A smaller number of temperature sensors is attached to a movable arm. It rotates stepwise around the cavity axis. The sensitivity of the moving sensors is not as high as in the fixed arrangement: the mechanical and thus the thermal contact of the sensor to the cavity wall is less reproducible and contact grease will be wiped off during movement. However, the location of a thermal instability (quench) and the heat produced by impinging field emitted electrons can be clearly detected. The rotating temperature mapping is widely used to localize heating effects in multicell structures.

In addition to the temperature sensors, small radiation detectors (diodes) are also placed around the cavity wall, being assembled on the same boards. They allow one to trace the trajectory of field emitted electrons by localizing the γ-radiation when impinging the inner cavity surface.

Temperature mapping is a suitable tool for localizing heating spots. However, some helpful information can be gained by pure radiofrequency measurements, avoiding any mechanical effort for diagnostics. In the case of multicell cavities it might be helpful to know which cell is troublesome, or if there is more than one possible quench location. An n-cell cavity has n different resonant frequencies, each having a well known radiofrequency excitation of the different cells (see equations (20) and (21)). The cavity behaviour can be measured in all n resonances. Hereby the quench limit and additional loss in each cell can be determined. Unfortunately, there is an ambiguity due to the mirror symmetry of a disc loaded waveguide with n cells: for an n-cell cavity, the mode measurement cannot differentiate between cell number x or $(n - x)$.

7. Fundamentals of cavity design

7.1. Principal cavity layout

Accelerating radiofrequency structures can be realized in different ways. There are three basic arrangements.

- Adding many individual cells of the same or nearly the same shape in a long arrangement. The input radiofrequency power is fed from one end of the structure and travels along with the particles to be accelerated. At the end of the structure the left-over radiofrequency power is coupled out and dissipated. This arrangement is named a travelling-wave structure and is realized in many normal conducting cases. The filling time of the structure is very fast, but high radiofrequency peak power is needed to establish a reasonable gradient (for a detailed analysis of travelling-wave structures see [41]).
- Only a few identical cells (typically up to ten) are coupled together. There is one input coupler, but this is not necessarily placed at one end of the structure. There is no second coupler to separate the remaining radiofrequency power. This arrangement is named a standing wave structure, because the radiofrequency wave is travelling back and forth in the accelerating structure. The cavity structure behaves as a resonator with its typical filling

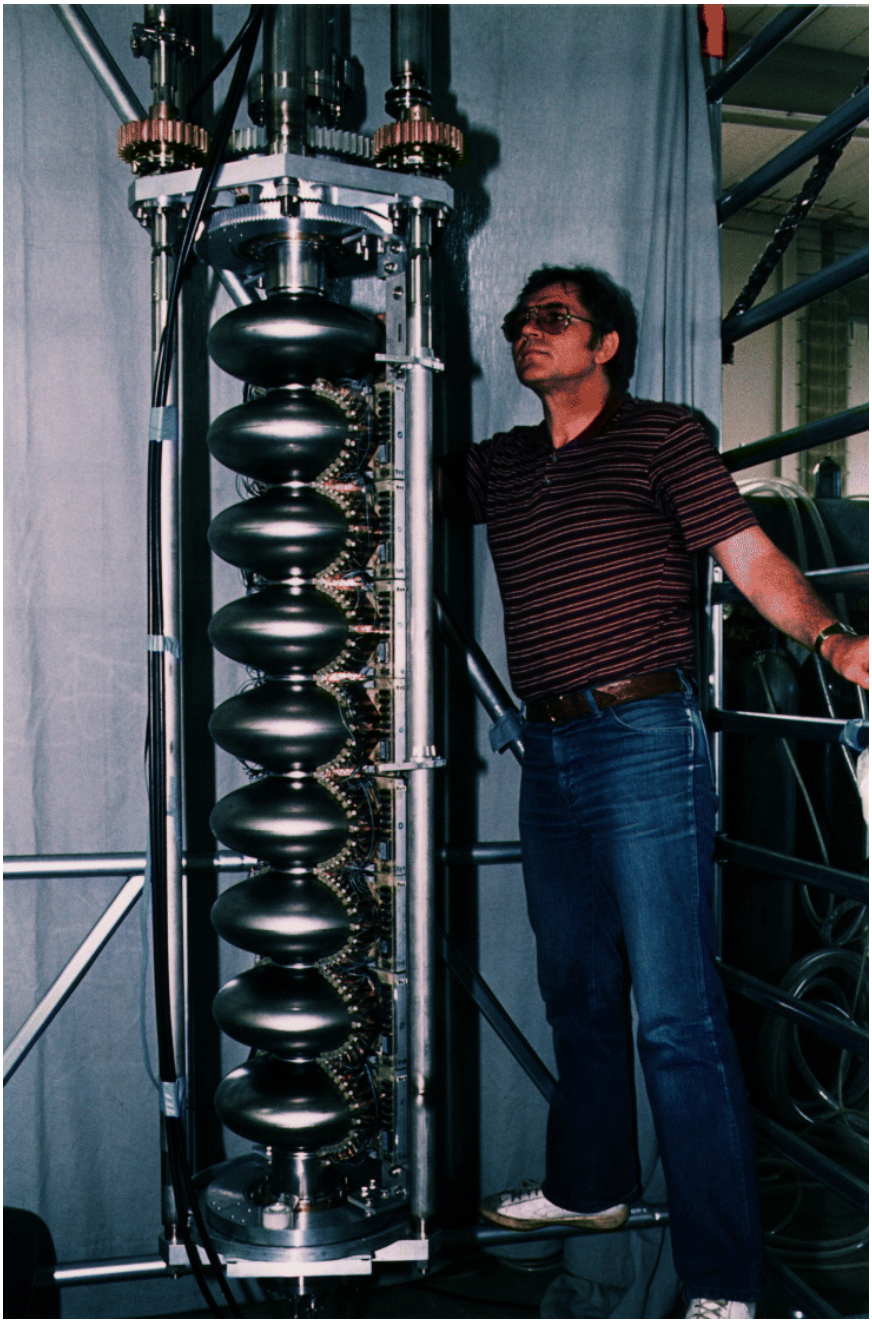

Figure 32. The temperature mapping system as a diagnostic tool to locate cavity areas of enhanced losses: carbon resistors are used as sensors to measure the temperature at the outer cavity wall. The resistors are placed on a movable arm which can be rotated around the cavity axis. In another design, fixed resistors are thermally bound to the cavity surface. Hereby a higher sensitivity is gained but many more sensors are needed for the same special resolution as with the rotating arrangement.

time, depending on the loss of the wall material. The 'forward' wave (forward means in the same direction as the particles to be accelerated) accelerates the synchronous particle, the backward wave has no effect on it. The advantage of this standing-wave arrangement is the reduced peak power demand because of the accumulative energy storage during filling. The backward wave will not contribute to the acceleration but will double the radiofrequency wall losses and the local surface fields. The standing-wave arrangement is in use for superconducting and normal conducting structures (for a detailed analysis of standing-wave structures see [41]).

• Only one resonating cell is fed by one radiofrequency input coupler. This single resonator arrangement is used in the case of very high beam current to reduce the input coupler power loading as well as to simplify the damping scheme for higher-order modes. It is also typically used for acceleration of particles with relative velocity β smaller than 1. The single-cell design is used for normal conducting and superconducting resonators.

The analysis of accelerating structures can be performed in two different approaches: resonant circuit analysis for the standing wave arrangement or space harmonic analysis for the travelling-wave case [41]. In the following sections the first method is applied, because all superconducting accelerating structures are operated in the standing-wave mode. There have been considerations of the use of travelling-wave arrangement because of its lower surface fields. The technical complexity of an external recirculation of the radiofrequency power, however, seems not worth the effort.

A standing-wave structure can be analysed as a chain of coupled resonators. Superconducting structures for $\beta = 1$ application consist of identical resonators (cells) with electric coupling. The end resonators (end cells) are slightly modified to compensate the missing coupling at the outer end. A chain of N coupled resonators has N different eigenmodes with N different amplitude relations. Under the simplifying assumption of electrical and only next-neighbour coupling the analysis results in solutions for the resonance frequencies and amplitudes as follows:

$$A_{n,q} = A \sin\left(\frac{\pi q(n-0.5)}{N}\right) \tag{20}$$

where $A_{n,q}$ is the field amplitude of cell n in mode q, A the normalized amplitude, q the mode number $1, 2, \ldots, N$ and n the cell number $1, 2, \ldots, N$,

$$\omega_q = \omega_0 \sqrt{\left(1 - \frac{k}{(1+2k)}\left(1 + \cos\frac{q\pi}{N}\right)\right)} \tag{21}$$

where ω_q is the resonance frequency of mode q, ω_0 the resonance frequency of one individual resonator and k the cell-to-cell coupling.

Equation (21) is the dispersion function of a chain of N coupled resonators, equation (20) describes the amplitude in cell number n when excited in mode number q. Figure 33 gives an example of the amplitude function of a three-cell resonator.

Superconducting accelerating structures for $\beta = 1$ application are excited in the so-called π-mode ($q = N$, so the argument in equation (20) is $\pm\pi$). All cells will be excited to the same amplitude but differ in phase by 180° (see figure 33(d)). The length of one cell is equal to 0.5 of the wavelength to obtain the synchronous condition between the radiofrequency wave and the particle to be accelerated. This mode has the highest efficiency for acceleration (= highest shunt impedance, see section 7.2) because each cell contributes to the acceleration with its maximum value.

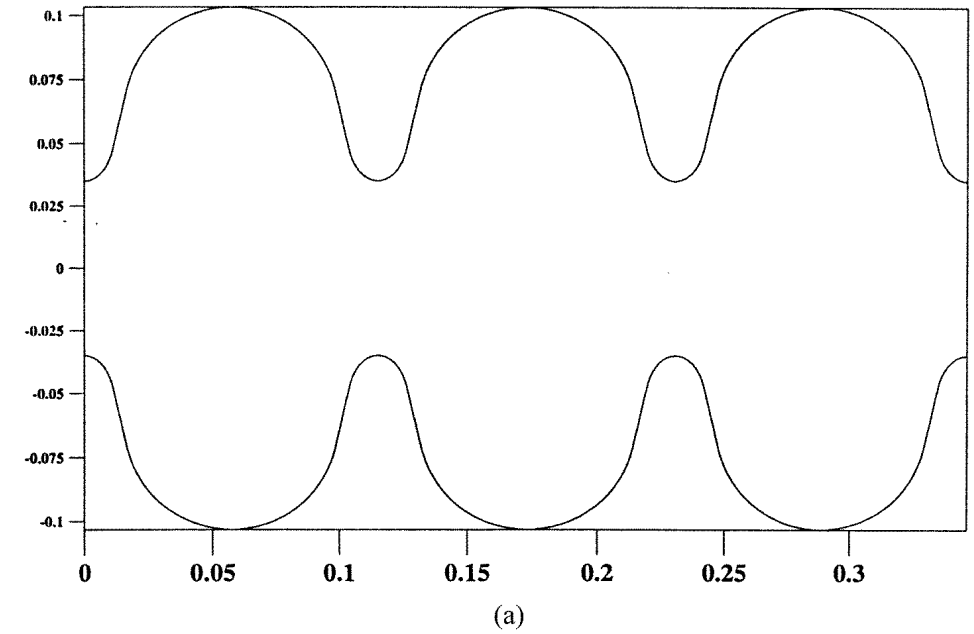

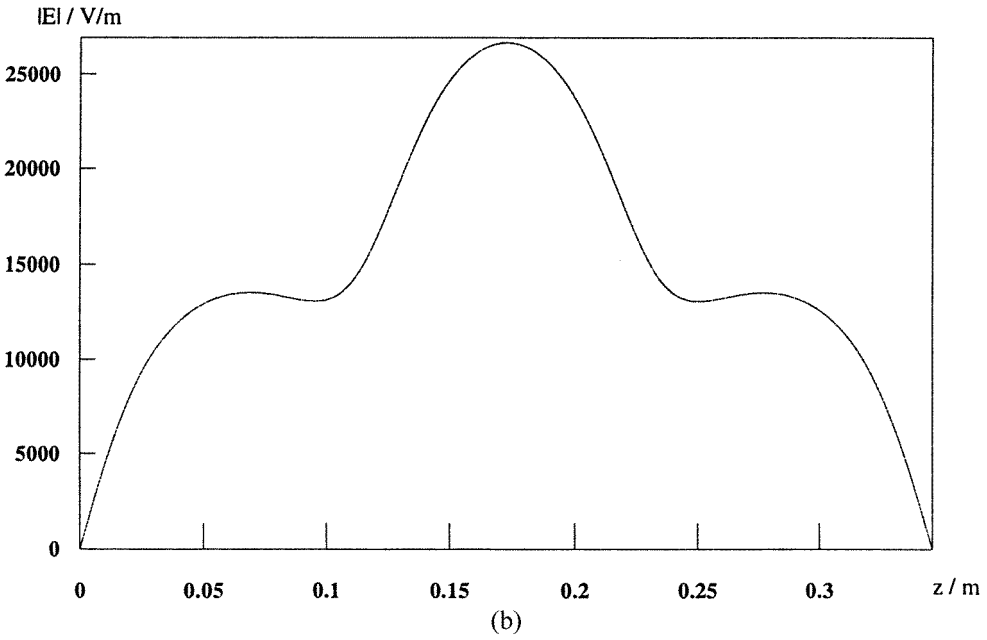

Figure 33. Excitation of a three-cell standing-wave accelerating resonator ($N = 3$, see equations (20) and (21)). The horizontal axis is the dimension along the beam axis, the vertical axis is the radial cavity dimension (a) and the relative amplitude of the accelerating voltage (b)–(d) along the beam axis. The structure will resonate at three different frequencies. The electric field along the axis is plotted for these resonances. (a) Cavity contour; (b) electric field of the lowest resonance; (c) electric field of the resonance at middle frequency; (d) electric field at the highest resonances used for acceleration.

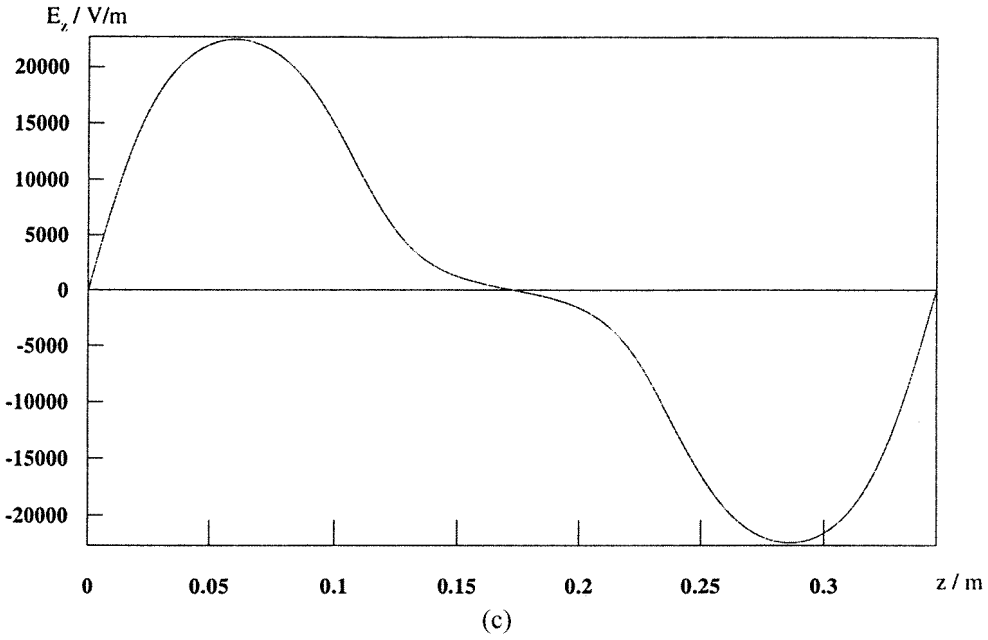

(c)

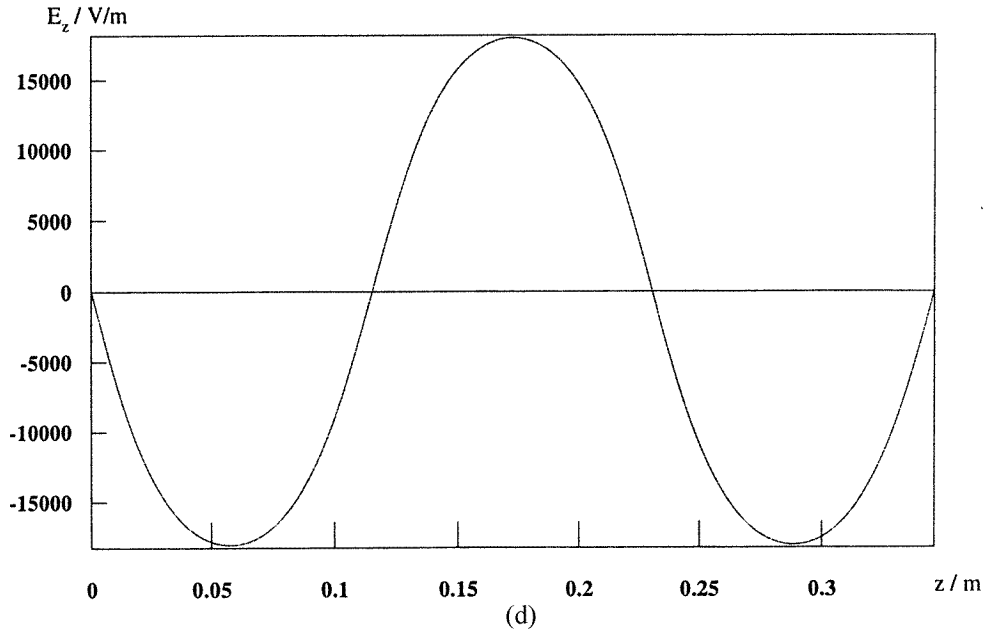

(d)

Figure 33. (Continued)

7.2. Shunt impedance, Q and R/Q value

The voltage drop across a resistor and its dissipated power is given by Ohm's law:

$$V^2 = 2 \cdot R \cdot P \tag{22}$$

where V is the peak voltage across a resistor R and P the power dissipated in the resistor R by an alternating current.

An 'Ohm's' law can be defined for a radiofrequency accelerating structure, accordingly:

$$U^2 = 2 \cdot R \cdot P \tag{23}$$

where U is the peak accelerating voltage seen by a particle when passing through the structure, P is the dissipated radiofrequency power in the structure to establish the voltage U, and R is the 'shunt impedance' of the accelerating structure.

In this definition the shunt impedance is the proportionality factor between the voltage squared and the dissipated power. It is a figure of merit, because it defines the power needed to establish the accelerating voltage U.

A resonating circuit stores energy. The Q-value is defined as the ratio of stored energy and dissipated power:

$$Q = \omega \times W/P \tag{24}$$

where Q is the quality factor, $\omega = 2\pi f$, W the stored energy and P the dissipated power.

A standard way to determine the quality factor is to measure the bandwidth of the resonance curve:

$$Q = \frac{f}{\delta f} \tag{25}$$

where f is the resonance frequency and δf the full width at half power points.

Superconducting cavities have quality factors in the range of 10^{10}. The equivalent bandwidth is less than 1 Hz. Therefore, it is more convenient to measure the quality factor by the decrement method:

$$Q = \omega \cdot \tau \tag{26}$$

where τ is the decay time constant of the stored energy.

Equation (23) can be rewritten as

$$U^2 = \frac{R}{Q} \cdot Q \cdot P. \tag{27}$$

In equation (27) the influence of geometry and material of the resonator is separated. To first order the Q-value will depend on the conductivity of the wall material only. Using equations (27) and (24), the R/Q-value is given by

$$\frac{R}{Q} = \frac{U^2}{\omega \cdot W}. \tag{28}$$

The accelerating voltage U is the line integral of the electric field along the axis of the resonator. The stored energy W is proportional to the volume integral of the square of the electric (or magnetic) field in the resonator. These fields are determined by Maxwell's equations and depend on the shape of the resonator and not on the conductivity of the wall material. It is, therefore, plausible that the value of R/Q reflects the geometry of the resonator.

7.3. Optimization considerations

In order to reduce the radiofrequency power demand, the product of $(R/Q)Q$ (equation (27)) must be maximized. The conductivity of the wall material determines the Q factor. Therefore, Cu is chosen in most cases for a normal conducting design. Shaping of the iris region is used to enhance the electric field strength on the cavity axis and thus to

enlarge R/Q. The range of improvement is limited, however, and typical cavity designs differ by not more than 20% in this respect. In the case of superconducting cavities a dramatic improvement is gained by the quality factor. Values of 5×10^9 are typical for niobium cavities in the GHz regime, whereas Cu resonators reach 5×10^4. Therefore, cavity shaping to improve the R/Q value is of less importance in the superconducting case.

In fact, the R/Q value is reduced on purpose in the superconducting case by a typical factor of two. The increase of the power needed to establish a given voltage U (see equation (27)) can be tolerated because of its very low absolute value (high Q!!). However, a reduction of the R/Q-value will considerably reduce the beam–cavity interaction strength. Hereby the excitation of higher frequencies by the beam current is lowered and beam instability requirements are relaxed.

The maximum accelerating gradients in a superconducting resonator are limited either by field emission or by a thermal instability. Therefore, the local surface electric and magnetic field should be reduced. This can be done by closing the iris diameter. On the other hand, the electric coupling to the next-neighbouring cells is diminished and the accelerating structure is more sensitive to mechanical tolerances. Therefore, the optimization of the superconducting cavity shape must be adopted to the individual operating conditions (see table 5).

Table 5. The effects and consequences of enlarging the iris diameter of a superconducting accelerating cavity.

Property	Effect	Consequence
R/Q of fundamental mode	Reduction	Can be tolerated because of high Q
R/Q of higher modes	Reduction	Will reduce beam instabilities
$E_{\text{peak}}/E_{\text{acc}}$	Enlargement	Will increase field emission
$H_{\text{peak}}/E_{\text{acc}}$	Enlargement	Will initiate thermal instability
Cell-to-cell coupling	Enlargement	Will relax mechanical tolerances

For example, beam stability is of great importance at high-beam-current accelerators. In this case the iris diameter should be large in order to reduce the beam–cavity interaction ('wake fields'). This is done at the cost of higher electric and magnetic surface fields. Fortunately, these cavities will not be operated at high gradients in this case. Because of the high beam current the gradient can only be moderate in order to keep the radiofrequency power (= accelerating voltage × beam current) at the input coupler at a manageable level.

If high gradients are of concern, however, the iris diameter should not be too large, otherwise the enhanced magnetic field will drive thermal instabilities or the enhanced electric field will initiate early field emission.

8. Conclusion

Superconducting cavities are in operation for electrons, positrons (velocity $\beta = 1$ design) and for (heavy) ions (velocity $\beta < 1$ design). High gradients, economical operation and favourable beam dynamics are the major advantages which drive the design of large-scale superconducting accelerators for future applications.

Niobium is the commonly used material for superconducting resonators. The performance of the best single-cell cavities comes close to the intrinsic limitation of the critical field of the bulk niobium. Large progress has been made in increasing Nb quality,

in the development of quality control in fabrication methods and in the improvement of handling procedures. Therefore, one can expect that high-gradient multicell structures will reach the same level of performance in the near future.

For high-current application, the gradient is determined by beam dynamics limitations or by radiofrequency power restrictions of auxiliary components. Resonators from bulk niobium or from niobium sputtered copper structures already meet the required performance. Auxiliary components (input and higher-order mode couplers, tuners, etc) need adequate care to perform with the required reliability.

Large-scale superconducting accelerating systems are under design or prototype development, such as the linear e^+e^- collider and proton accelerators. Progress is expected in simplifying production methods thus reducing investment costs.

Acknowledgments

The support of my colleagues in the superconducting cavity community by stimulating discussions and the supply of data and figures is greatly acknowledged. Special thanks are given to V Palmieri for providing material on low β cavities and to P Schmueser for critical reading of the manuscript and valuable comments.

References

[1] Brinkmann R, Materlik G, Rossbach J and Wagner A (eds) 1997 Conceptual design of a 500 GeV e^+e^- linear collider with integrated x-ray laser facility *Internal Report* DESY 1997-048, ECFA 1997-182
[2] Padamsee H, Knobloch J and Hays T 1998 *RF Superconductivity for Accelerators* (New York: Wiley) to be published
[3] Noguchi S *et al* 1994 *Proc. 4th EPAC (London)* vol 3 (Singapore: World Scientific) pp 1891–3
[4] Dwersteg B *et al* 1994 *Proc. 4th EPAC (London)* vol 3 (Singapore: World Scientific) pp 2039–41
[5] Reece C *et al* 1995 *Proc. 1995 IEEE PAC (Dallas)* p 1512
[6] Cauvin B *et al* 1989 *Proc. 1989 Part. Acc. Conf. (Chicago), IEEE Trans. Nucl. Sci.* **NS-1** 601
[7] Cavallari G *et al* 1994 *Proc. 4th EPAC (London)* vol 3 (Singapore: World Scientific) pp 2042–4
[8] Boussard D *et al* 1989 *Proc. of Natl Acc. Conf. (Chicago)* vol 3, p 1783
[9] Edwards D (ed) 1995 *TESLA Test Facility Design Report* DESY, TESLA-Report 95-01
[10] Calarco J R *et al* 1977 *IEEE Trans. Nucl. Sci.* **NS-24** 1091
[11] Axel P *et al* 1977 *IEEE Trans. Nucl. Sci.* **NS-24** 1133
[12] Doebert S *et al* 1994 *Proc. 4th EPAC (London)* vol 1 (Singapore: World Scientific) pp 719–21
[13] Pardo R C *et al* 1993 *Proc. 1993 IEEE PAC (Washington)* vol 3 (IEEE Catalog) pp 1694–9
[14] Noe J W 1986 *Rev. Sci. Instrum.* **57** 757
[15] Fox J D 1986 *Rev. Sci. Instrum.* **57** 763
[16] Amsbaugh J F *et al* 1986 *Rev. Sci. Instrum.* **57** 761
[17] Shibata M 1993 *Proc. 6th SRF Workshop (Newport News)* vol 1, ed R Sundelin (Newport News, VA: CEBAF) pp 124–30
[18] Fortuna G and Pengo R *et al* 1990 The Alpi project at the Laboratori Nazionali di Legnaro *Nucl. Instrum. Methods* A **287** 253
[19] Weisser D C 1993 *Proc. 6th SRF Workshop (Newport News)* vol 1, ed R Sundelin (Newport News, VA: CEBAF) p 26
[20] Benvenuti C *et al* 1991 *Proc. IEEE Part. Accelerat. Conf. (San Francisco)* vol 2 (New York: IEEE) p 1023
[21] Mueller G *et al* 1996 *Proc. 5th EPAC (Sitges)* vol 2 (Bristol: IOP Publishing) p 1645
[22] Padamsee H, Shepard K W and Sundelin R 1993 *Ann. Rev. Nucl. Sci.* **43** 635–86
[23] Kneisel P 1988 *J. Less-Common Met.* **139** 179
[24] Safa H, Moffat D, Bonin B and Koechlin F 1996 *J. Alloys Compounds* **232** 281
[25] Mueller G 1988 *Proc. 3rd SRF Workshop (Argonne)* vol 1, ed K W Shepard, ANL-PHY-88-1, pp 331–58
[26] Kneisel P and Lewis B 1996 *Part. Accelerat.* **53** 97–121
[27] Singer W, Proch D and Brinkmann A 1997 *Proc. 8th SRF Workshop on Particle Accelerators* to be published
[28] Mahner E *et al* 1993 *Appl. Surf. Sci.* **67** 23

[29] Tan J 1996 *Particle Accelerators* **53/54** 1–34
[30] Weingarten W 1996 *Particle Accelerators* **53/54** 199–215
[31] Bednorz J G and Mueller K A 1986 *Z. Phys* B **64** 189
[32] Hein A M 1996 *Particle Accelerators* **53/54** 135
[33] Rode C and Proch D 1990 *Proc. 4th SRF Workshop (KEK Tsukuba)* vol 2, ed Y Kojima *KEK Report* 89-21, pp 751–3
[34] Bardeen J, Cooper L N and Schrieffer 1957 *Phys. Rev.* **108** 1175
[35] Arnolds G and Proch D 1977 *IEEE Trans. Magn.* **MAG-13** 500
[36] Yogi T, Dick G J and Mercereau J E 1977 *Phys. Rev. Lett.* **39** 826
[37] Vallet C *et al* 1992 *Proc. 3rd EPAC (Berlin)* vol 2 (Gif-sur-Yvette: Editions Frontieres) pp 1295–7
[38] Saito K and Kneisel P 1992 *Proc. 3rd EPAC (Berlin)* vol 2 (Gif-sur-Yvette: Editions Frontieres) p 1231
[39] Fowler R H and Nordheim L 1928 *Proc. Roy. Soc.* A **119** 173
[40] Klein U and Proch D 1979 *Proc. Conf. Future Possibilities for Electron Accelerators (Charlottesville, VA)* ed J S McCarthy and R R Whitney N1-N17
Lagomarsino V *et al* 1979 *IEEE Trans. Mag.* **MAG-15** 25
[41] Lapostolle P and Septier A L 1970 *Linear Accelerators* (Amsterdam: North-Holland)
[42] Blaschke R 1981 *Recent Developments in Condensed Matter Physics* vol 4, ed J T Devreese *et al* (New York: Plenum) p 425
[43] Belomestnykh S *et al* 1996 *Proc. 5th EPAC (Sitges)* vol 2 (Bristol: IOP Publishing) p 2100